Electronic Supplementary Material (ESI) for Organic & Biomolecular Chemistry.

Electronic Supporting Information

β-Amyrin synthase from *Euphorbia tirucalli* L. Functional analyses of the highly conserved aromatic residues Phe413, Tyr259 and Trp257 disclose the importance of the appropriate steric bulk, and cation-π and CH-π interactions for the efficient catalysis of the polyolefin cyclization cascade

Ryousuke Ito, Chika Nakada and Tsutomu Hoshino*

Graduate School of Science and Technology and Department of Applied Biological Chemistry, Faculty of Agriculture, Niigata University, Ikarashi 2-8050, Nishi-ku, Niigata 950-2181, Japan

Figure S1. Amino acid alignment of various oxidosqualene cyclases

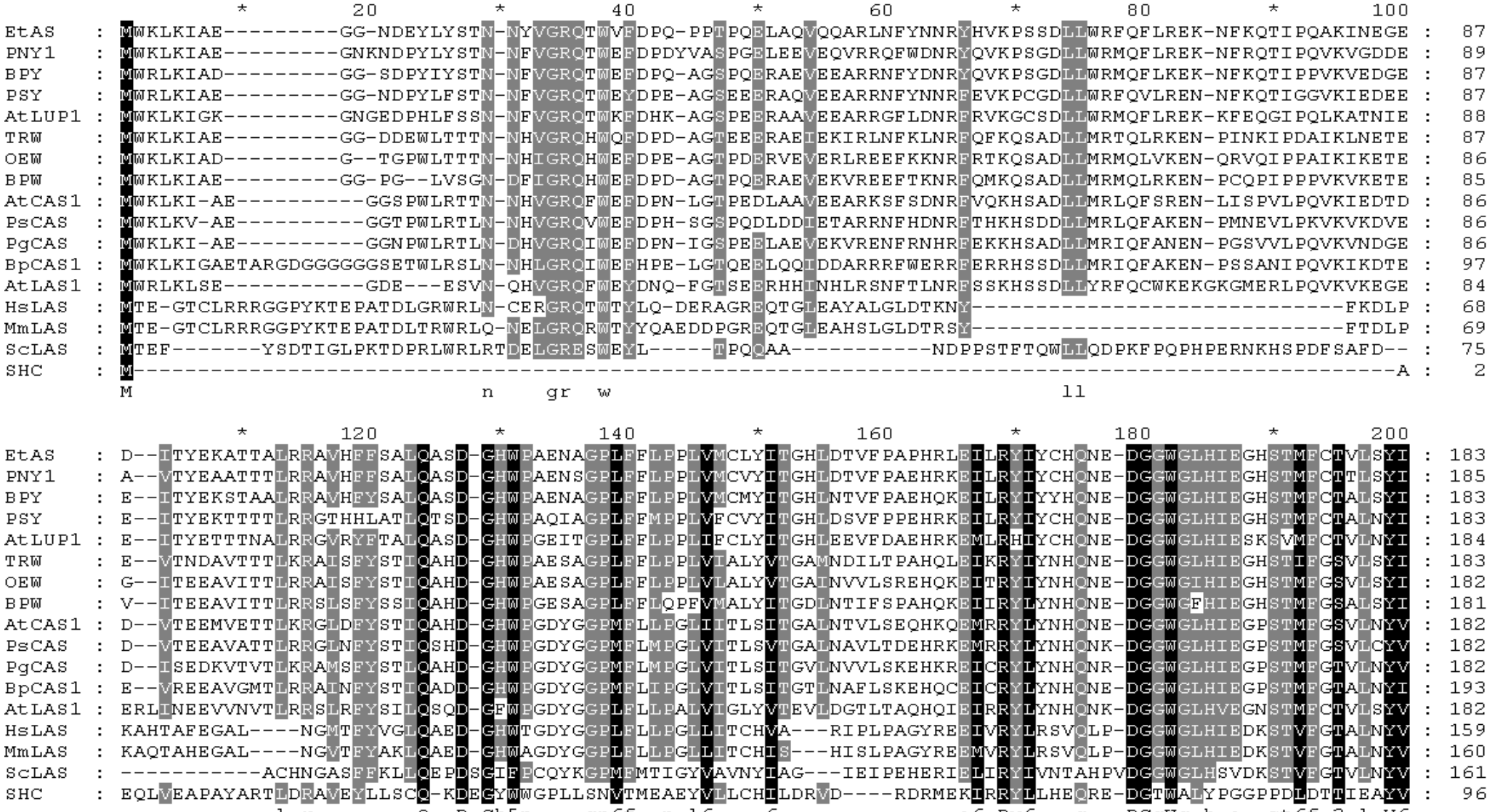

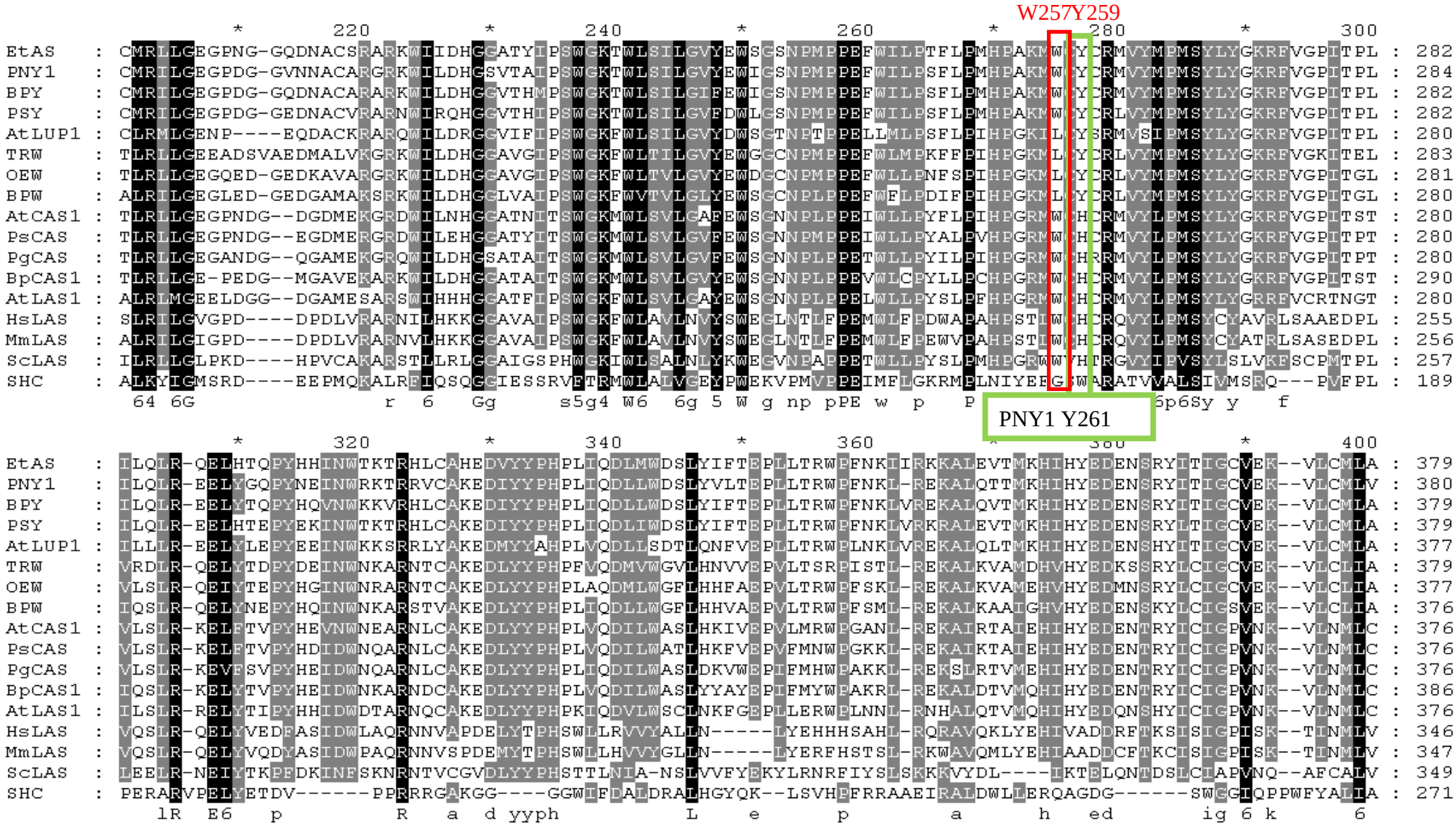
W257Y259
PNY1 Y261

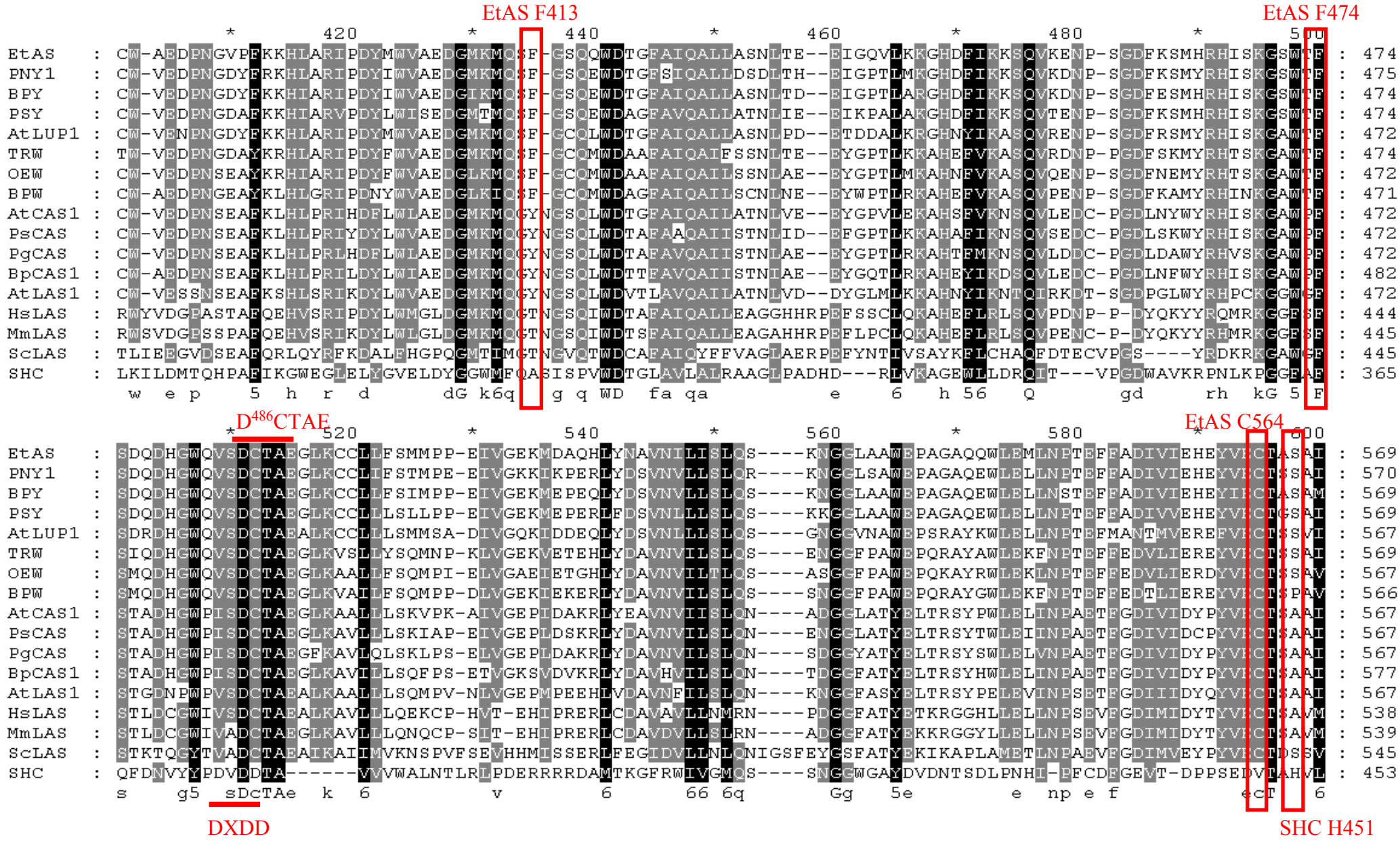

D485C486TAE involved in EtAS β-amyrin synthase

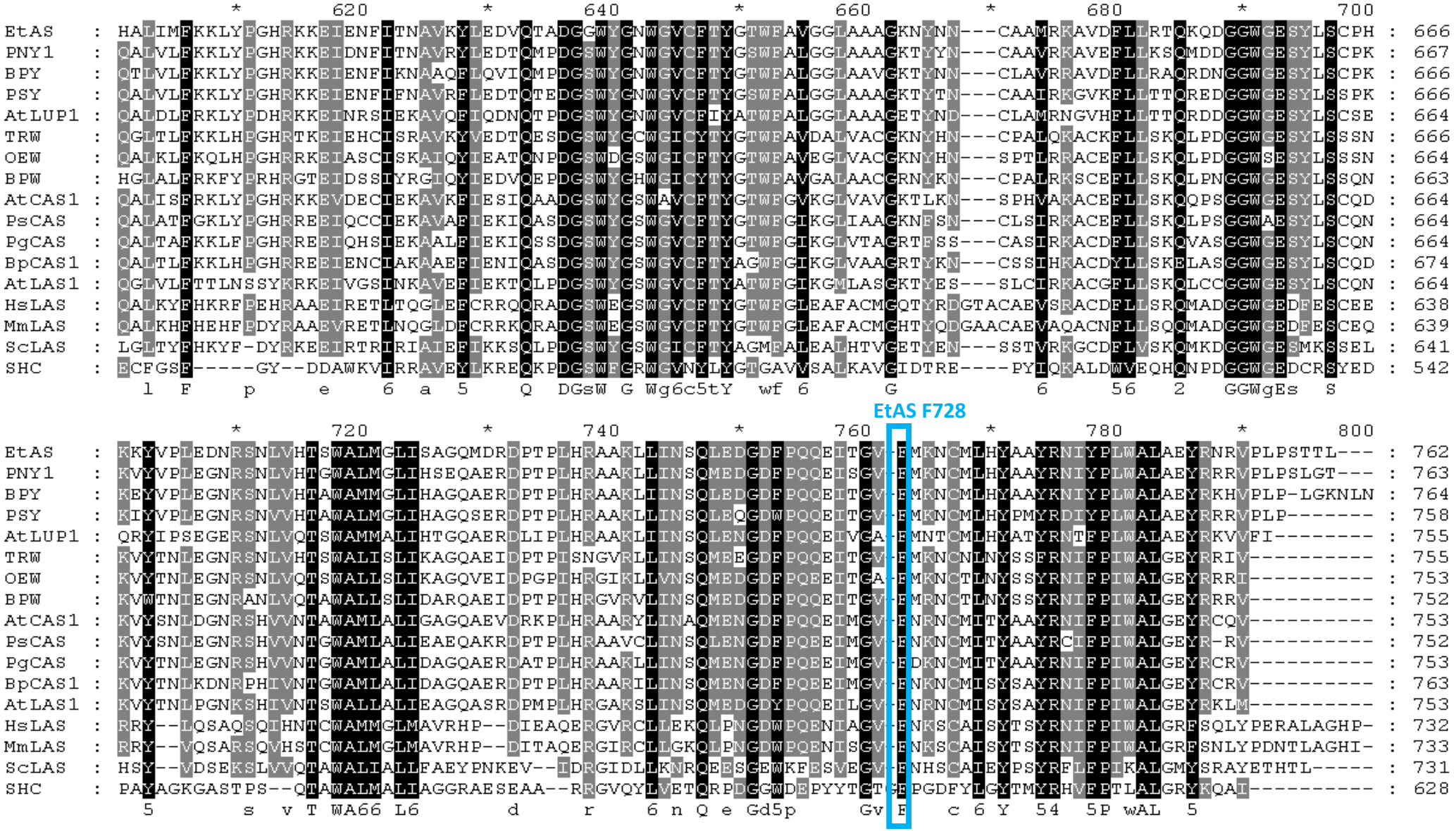
EtAS F728

```
                 *
EtAS    : --------------- :   -
PNY1    : --------------- :   -
BPY     : QVVNCIGQSLYKKYK : 779
PSY     : --------------- :   -
AtLUP1  : -------------VN : 757
TRW     : ----------QNI-- : 758
OEW     : ----------LHAQT : 758
BPW     : ----------LFA-- : 755
AtCAS1  : ---------LLQQGE : 759
PsCAS   : ---------L--QAC : 756
PgCAS   : ---------L-QGPS : 758
BpCAS1  : ---------L--KAL : 767
AtLAS1  : ---------L---SL : 756
HsLAS   : --------------- :   -
MmLAS   : --------------- :   -
ScLAS   : --------------- :   -
SHC     : ------------ERR : 631
```

The triterpene cyclases amino acids sequences were aligned using Clustal W, as implemented in the (CLC Sequence Viewer (CLC bio), and the figure was made by GenDoc (http://www.nrbsc.org/gfx/genedoc/). EtAS: *Euphorbia tirucalli* β-amyrin synthase (AB206469), PNY1: *Panax ginseng* β-amyrin synthase (AB009030), BPY: *Betula platyphylla* β-amyrin synthase (AB055512), PSY: *Pisum sativum* β-amyrin synthase (AB034802), AtLUP1: *Arabidopsis thaliana* multifunctional triterpene cyclase (At1g78970), TRW: *Taraxacum officinale* lupeol synthase (AB025345), OEW: *Olea europaea* lupeol synthase (AB025343), BPW: *Betula platyphylla* lupeol synthase (AB055511), AtCAS1: *Arabidopsis thaliana* cycloartenol synthase (At2g07050), PsCAS: *Pisum sativum* cycloartenol synthase (D89619), PgCAS: *Panax ginseng* cycloartenol synthase (AB009029), BpCAS1: *Betula platyphylla* cycloartenol synthase (AB055509), AtLAS1: *Arabidopsis thaliana* lanosterol synthase (At3g45130), HsLAS: *Homo sapiens* lanosterol synthase (P48449), MmLAS: *Mus musculus* lanosterol synthase (AK044016), ScLAS: *Saccharomyces cerevisiae* lanosterol synthase (P38604), SHC: *Alicyclobacillus acidocaldarius* squalene-hopene cyclase

Fig. S2. EIMS and NMR spectra of Product **10**-acetate

Fig. S2-1. EIMS spectrum of Product **10** acetate

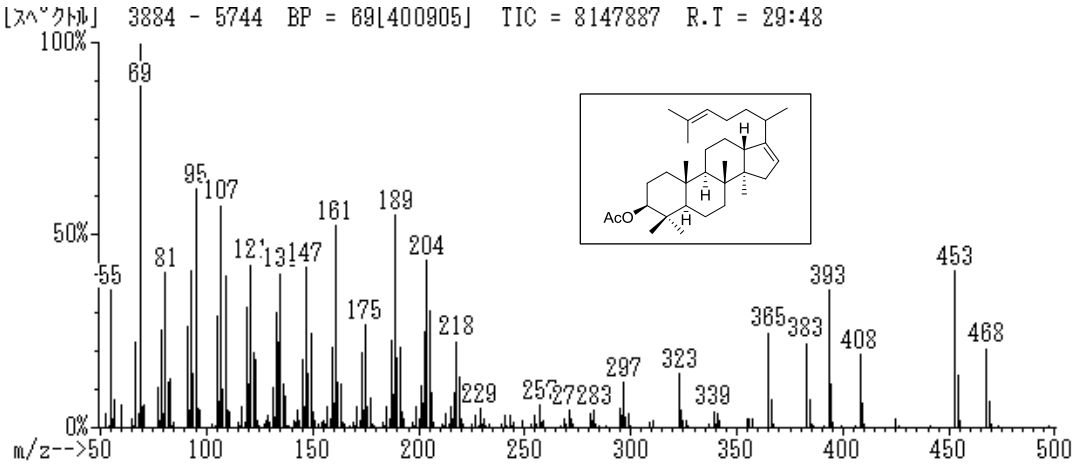

Fig. S2-2. ^{1}H-NMR spectrum of product **10**-Ac in $CDCl_3$ (600 MHz).

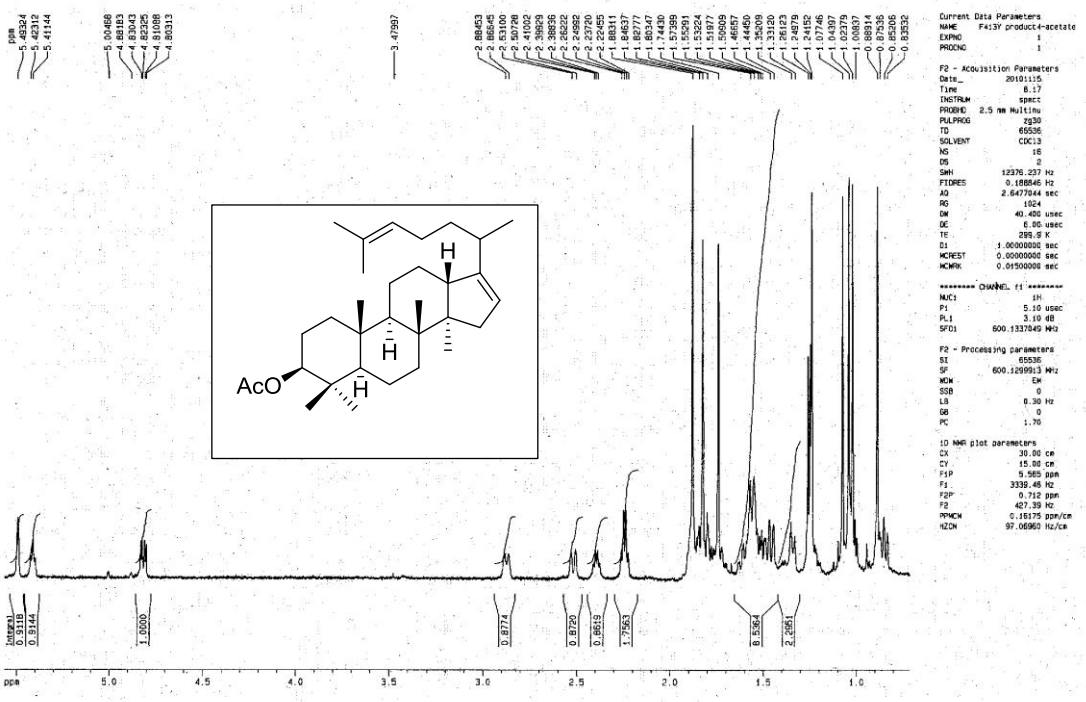

Fig. S2-3. ^{13}C-NMR spectrum of product **10** Ac (150 MHz)

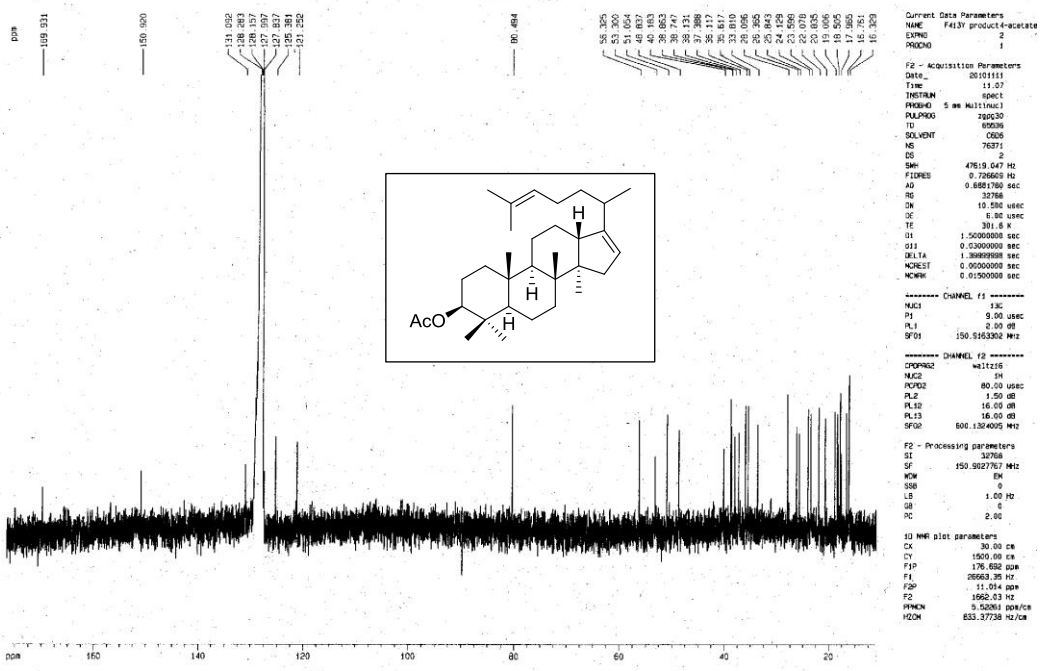

Fig. S2-4. ^{1}H-^{1}H COSY 90 of product **10** Ac

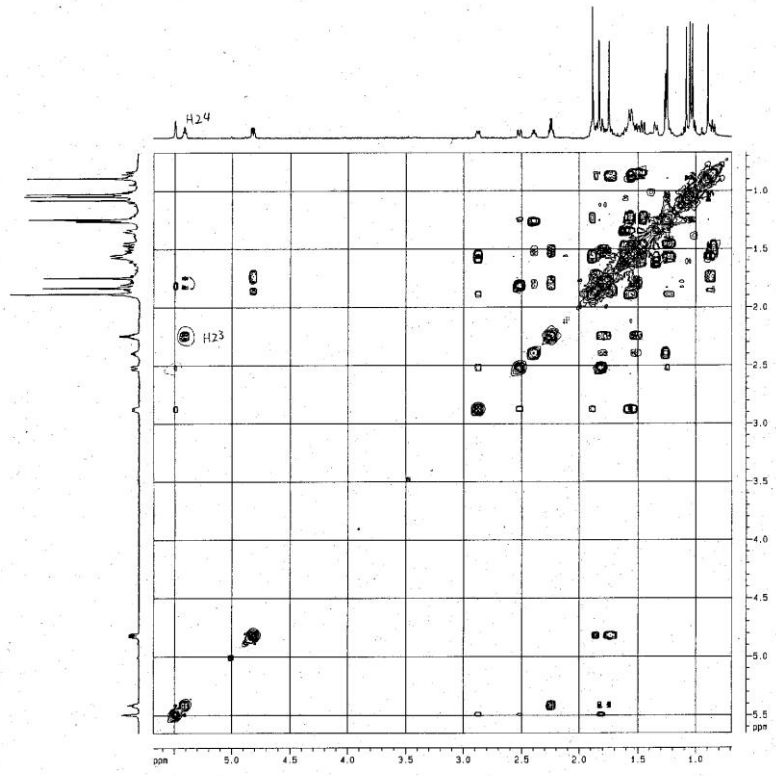

Fig. S2-5. HOHAHA spectrum of product **10** Ac

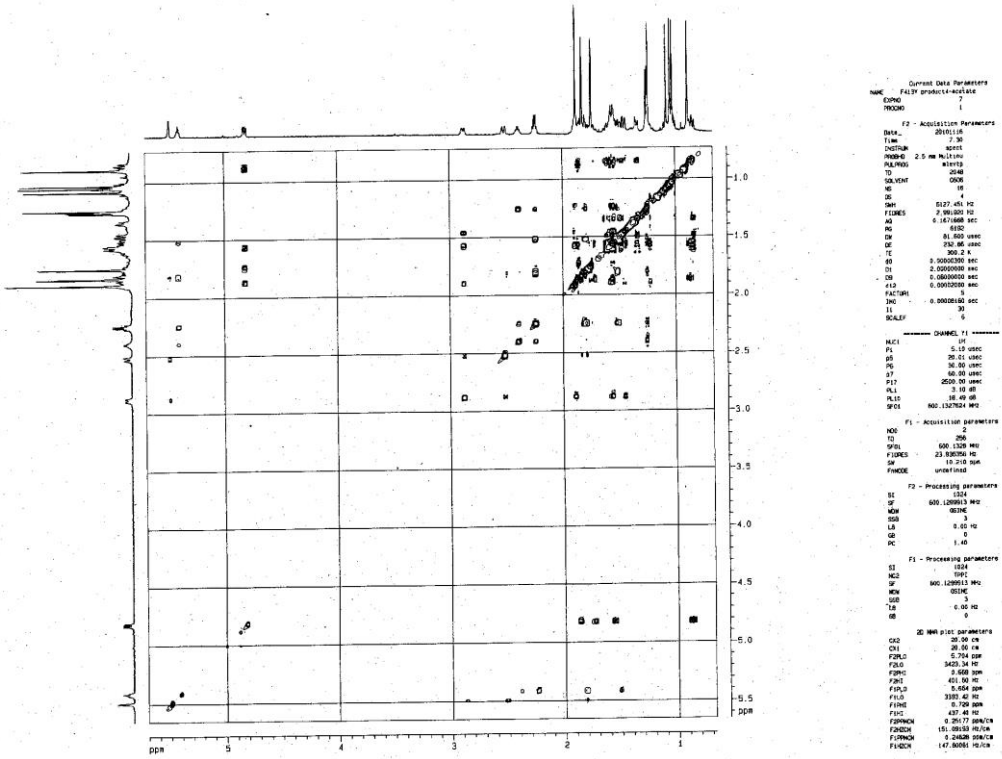

Fig. S2-6. NOESY spectrum of product **10** Ac

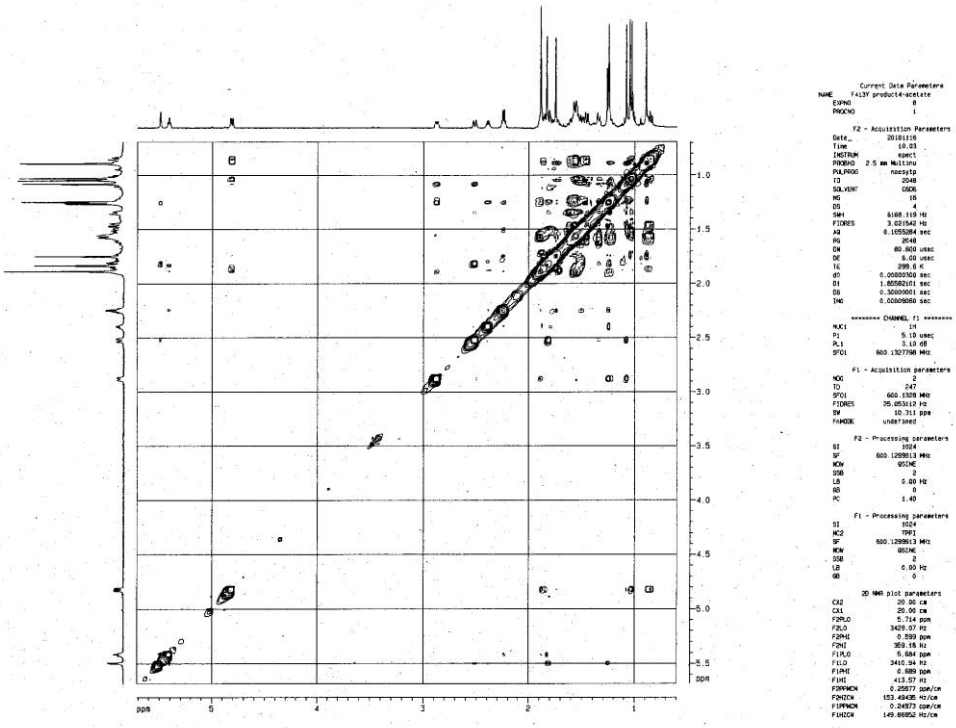

Fig. S2-7. HSQC spectrum of product **10** Ac

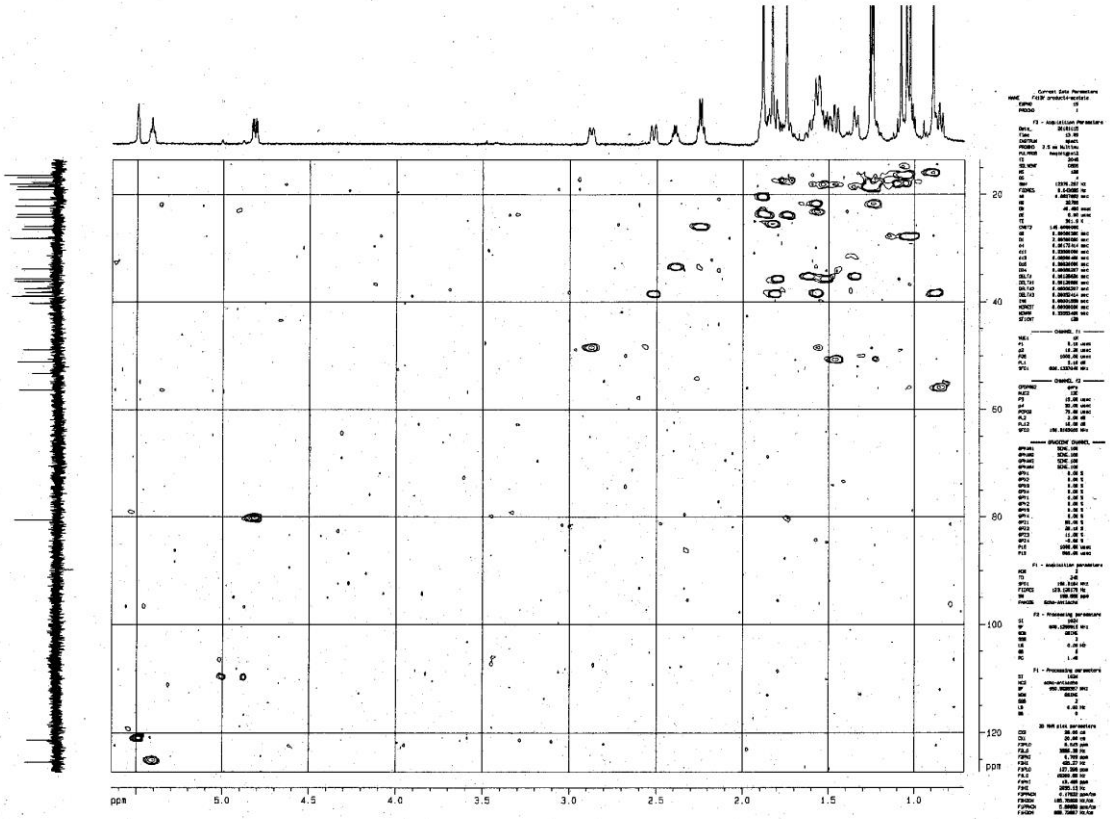

Fig. S2-8. HMBC spectrum of product **10** Ac

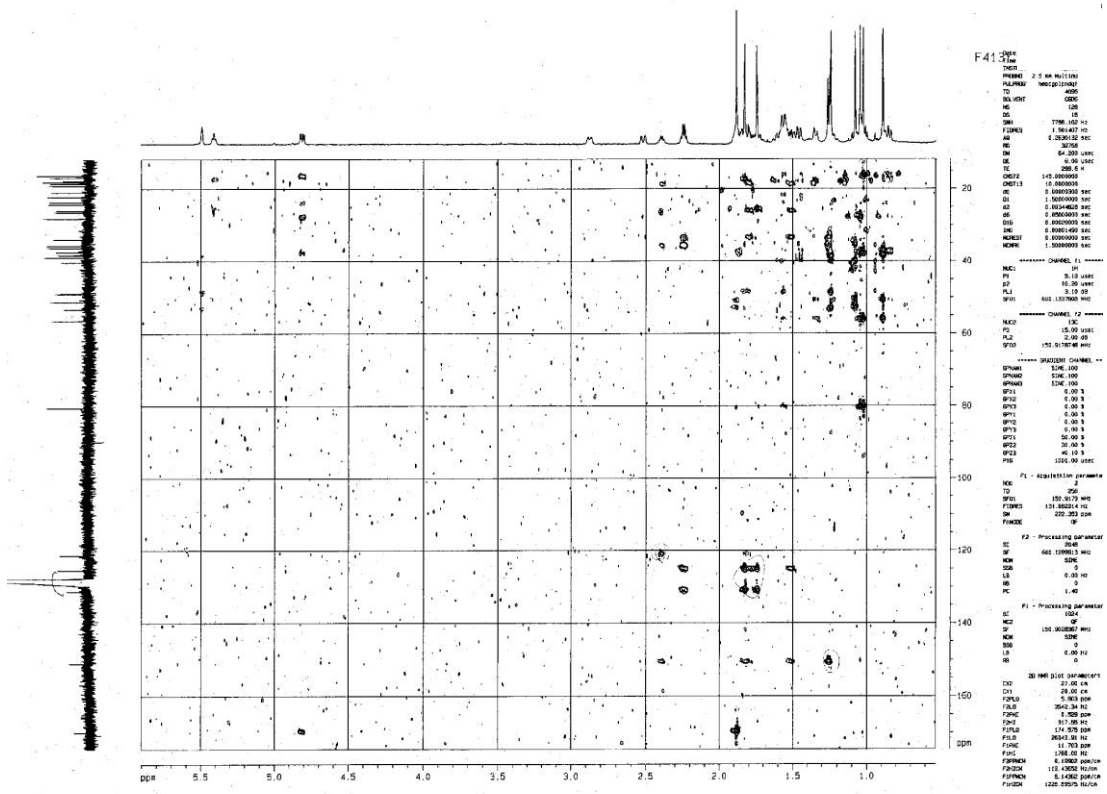

Fig. S2-9. NMR data analyses for proposing structure of **10**-Ac, optical rotation and HRMS data.

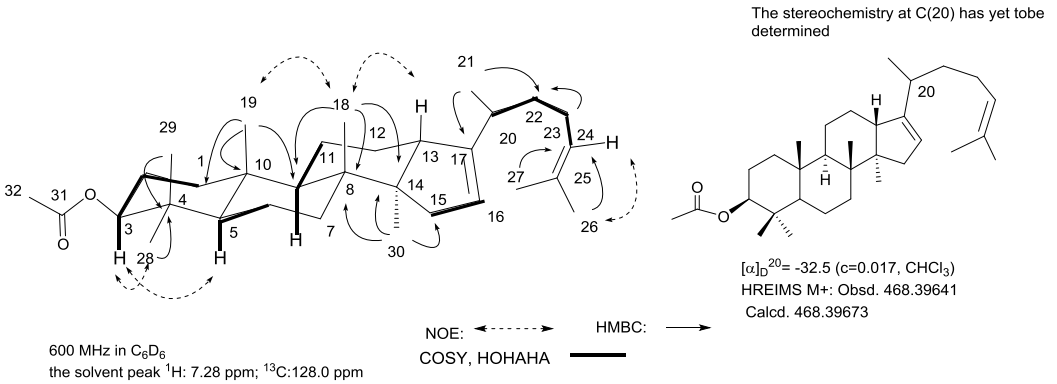

NO.	^{1}H	^{13}C	NO.	^{1}H	^{13}C	NO.	^{1}H	^{13}C	NO.	^{1}H	^{13}C
1	0.88(m);1.57(m)	38.75	9	1.456 (bd, J=12.5 Hz)	51.05	17	——	150.9	25	——	131.1
2	1.75(m);1.86(m)	24.13	10	——	37.39	18	1.077(3H,s)	18.34	26	1.827(3H, s)	25.84
3	4.81 (dd, J=11.7, 4.6Hz)	80.49	11	1.24(m);1.58(m)	22.08	19	0.889(3H, s)	16.33	27	1.744(3H,s)	17.71
4	——	38.13	12	1.57(m);1.89(m)	23.60	20	2.394(q, J=6.6 Hz)	33.81	28	1.024(3H, s)	28.09
5	0.844 (bd, J=10.1 Hz)	56.33	13	2.875(bd, J=10.9Hz)	48.84	21	1.256(3H, d, J=6.8 Hz)	19.01	29	1.044(3H, s)	16.76
6	1.46(m);1.58(m)	18.50	14	——	53.30	22	1.51(m);1.80(m)	36.12	30	1.241(3H, s)	17.96
7	1.35(m);1.62(m)	35.62	15	1.81(m);2.52(bd, J=14.0Hz)	38.86	23	2.24(dt,, J=7.3, 7.3 Hz)	26.36	31	——	169.9
8	——	40.18	16	5.49(bs)	121.2	24	5.41(t, 7.0 Hz)	125.4	32	1.883(3H, s)	20.83

The stereoisomer of **10**, described below, was isolated by Wu's group from the mutants of S. cerevisiae lanosterol synthase, which was reported in the following references.

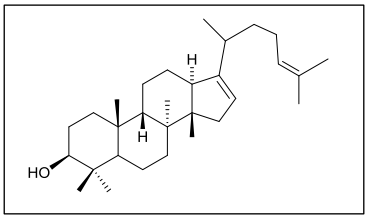

1. Wu, Tung-Kung; Chang, Yi-Chun; Liu, Yuan-Ting; Chang, Cheng-Hsiang; Wen, Hao-Yu; Li, Wen-Hsuan; Shie, Wen-Shiang, Organic & Biomolecular Chemistry (2011), 9(4), 1092-1097.

2. Liu, Yuan-Ting; Hu, Tain-Chang; Chang, Cheng-Hsiang; Shie, Wen-Shiang; Wu, Tung-Kung, Organic Letters (2012), 14(20), 5222-5225.

Fig. S3. EIMS and NMR spectra of Product **12**-acetate.

Fig. S3-1. EIMS spectrum of product **12**-Ac

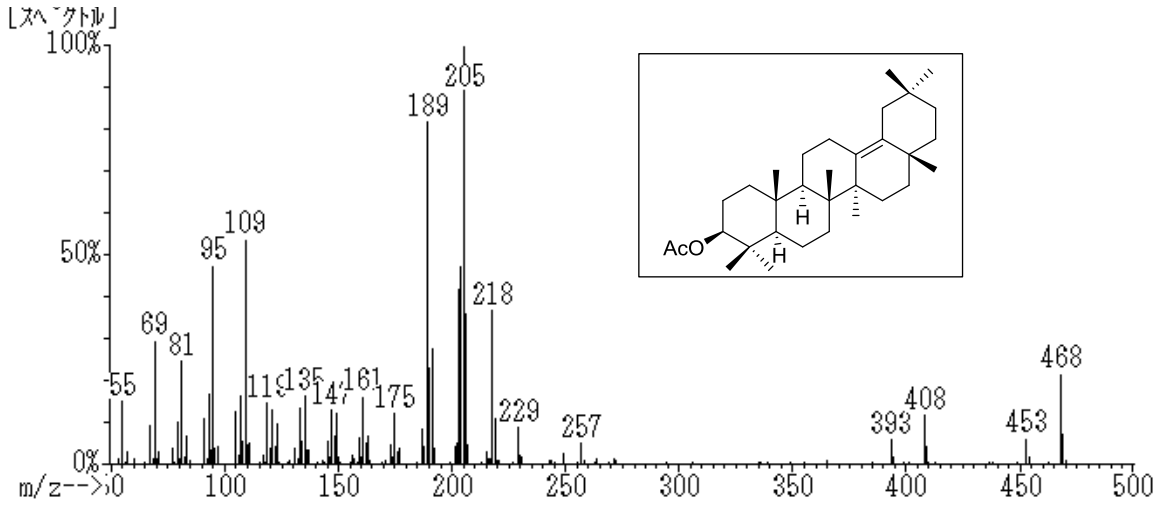

Fig. S3-2. ^{1}H-NMR spectrum of product **12**-Ac in C_6D_6 (400 MHz).

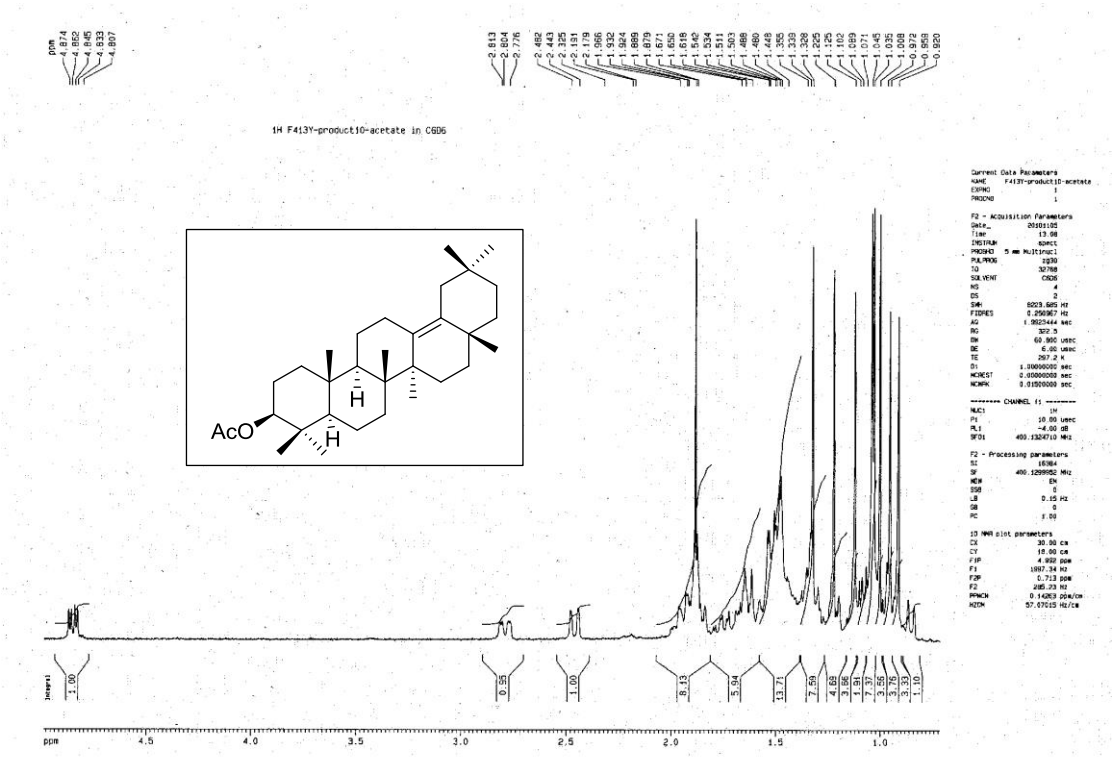

Fig. S3-3. ^{13}C-NMR spectrum of product **12**-Ac in C_6D_6 (100 MHz).

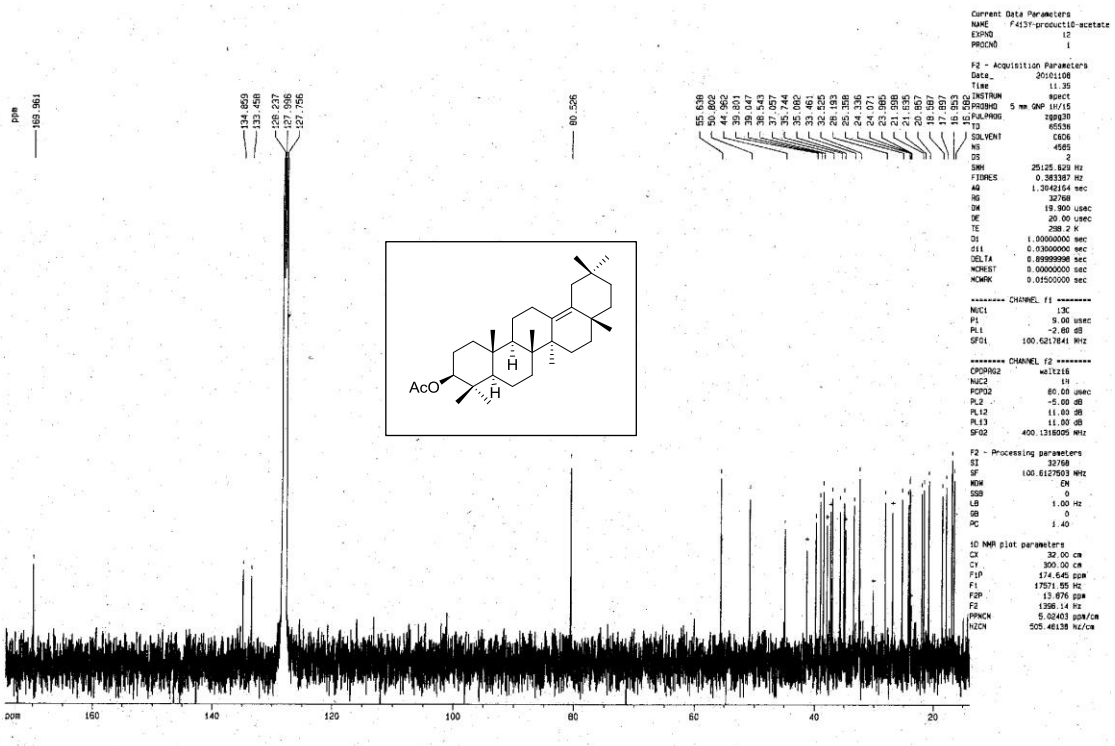

Fig. S3-4. ^{1}H-^{1}H COSY spectrum of product **12**-Ac in C_6D_6.

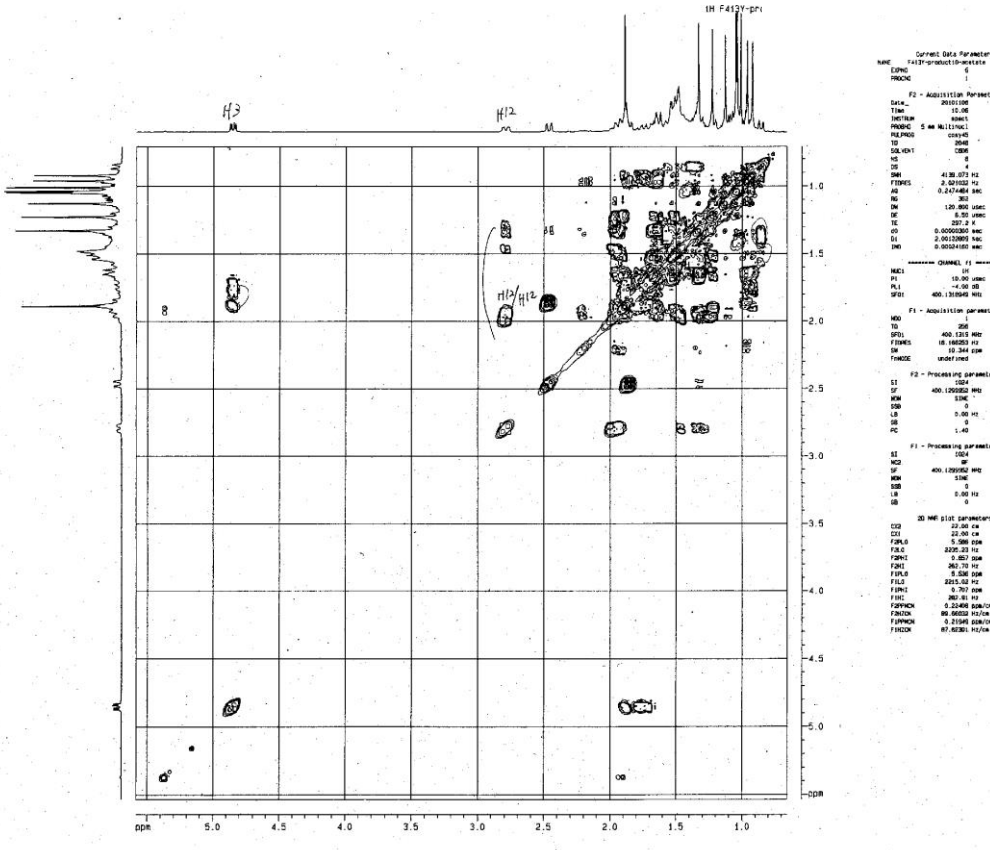

Fig. S3-5. HOHAHA spectrum of product **12**-Ac in C_6D_6.

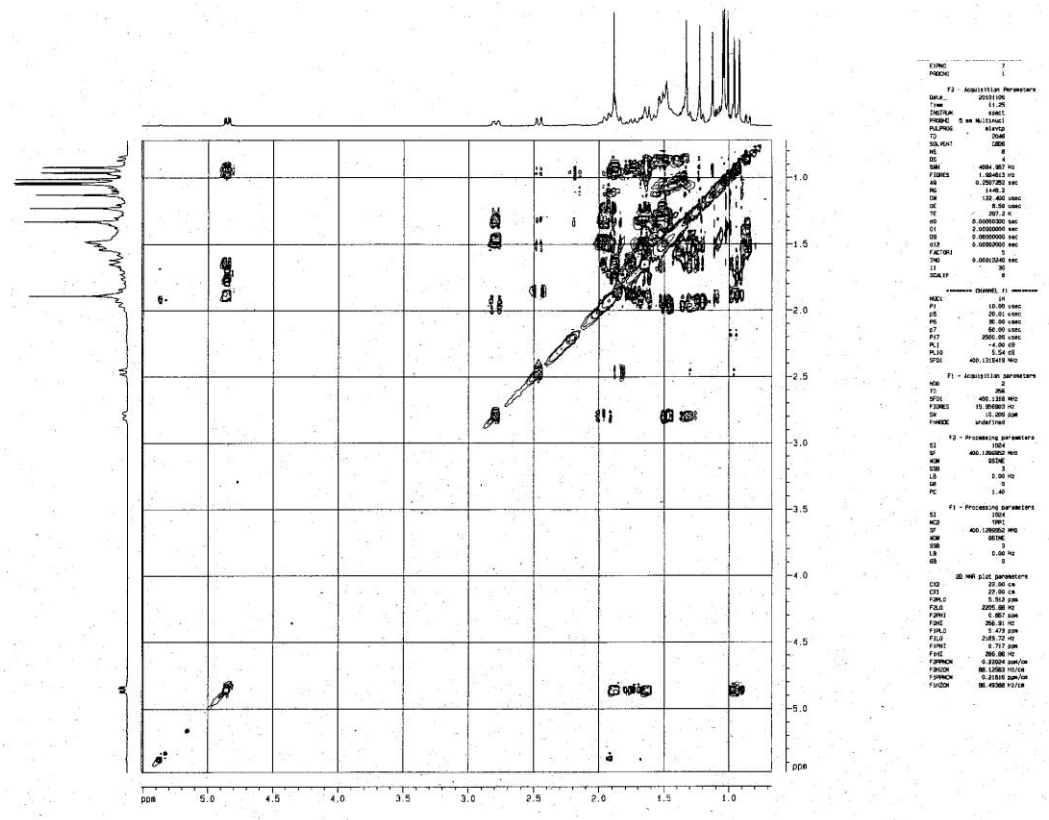

Fig. S3-6. NOESY spectrum of product **12**-Ac in C_6D_6 (400 MHz).

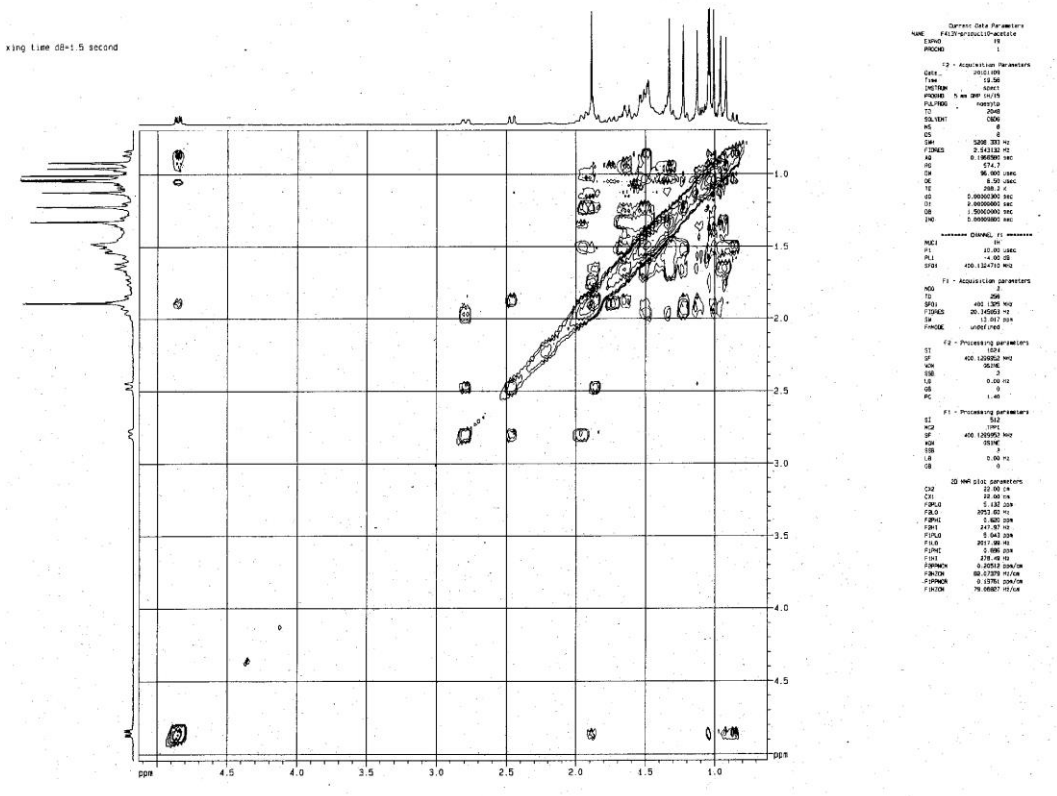

Fig. S3-7. NOESY spectrum of product **12**-Ac in C_6D_6 (600 MHz)-Expanded Region)

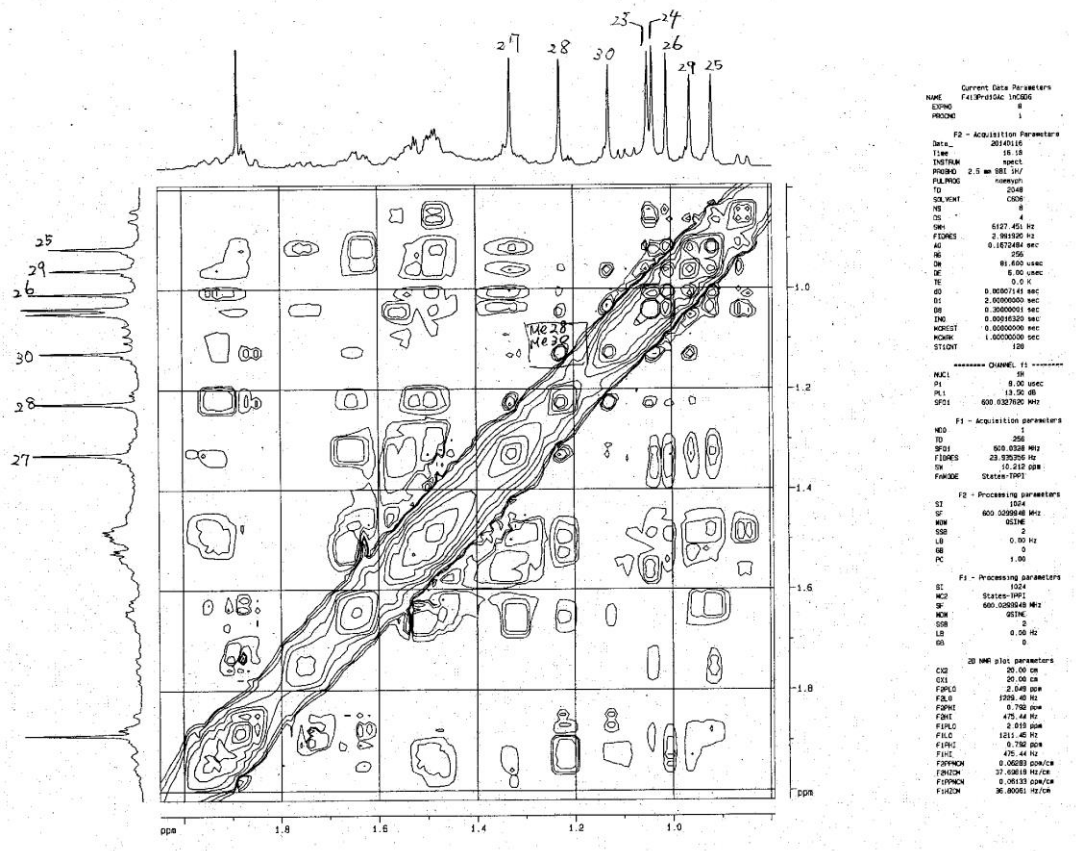

Fig. S3-8. HSQC spectrum of product **12**-Ac in C_6D_6

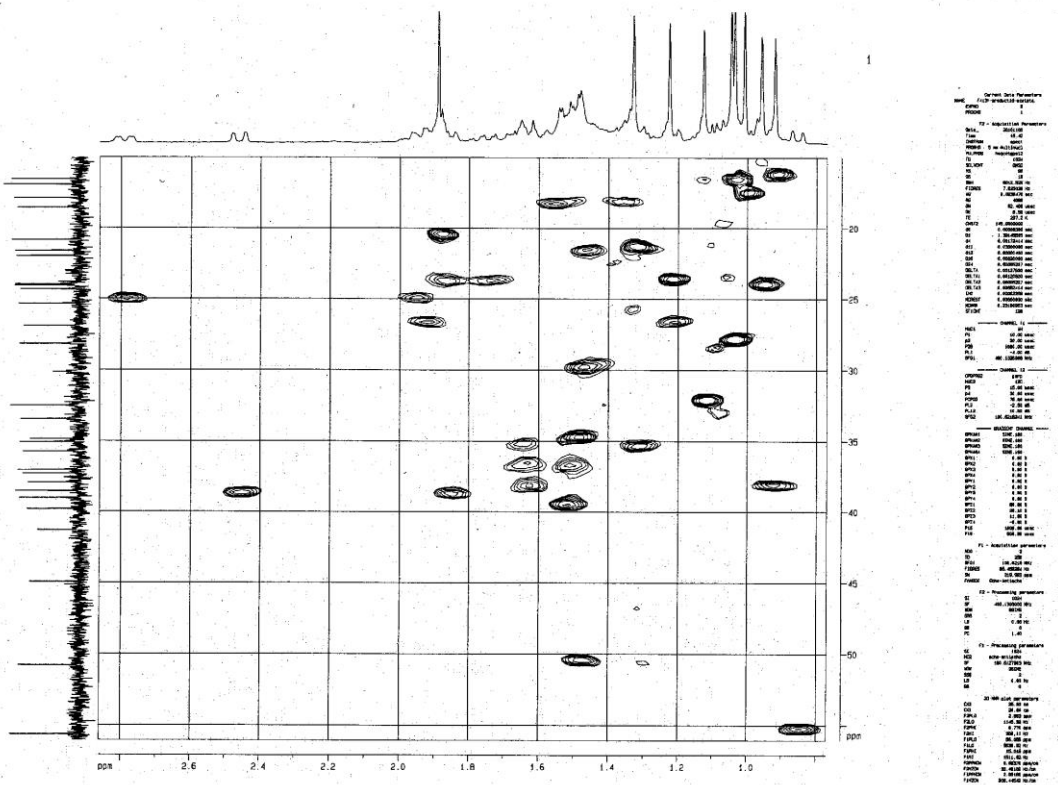

Fig. S3-9. HMBC spectrum of product **12**-Ac in C_6D_6

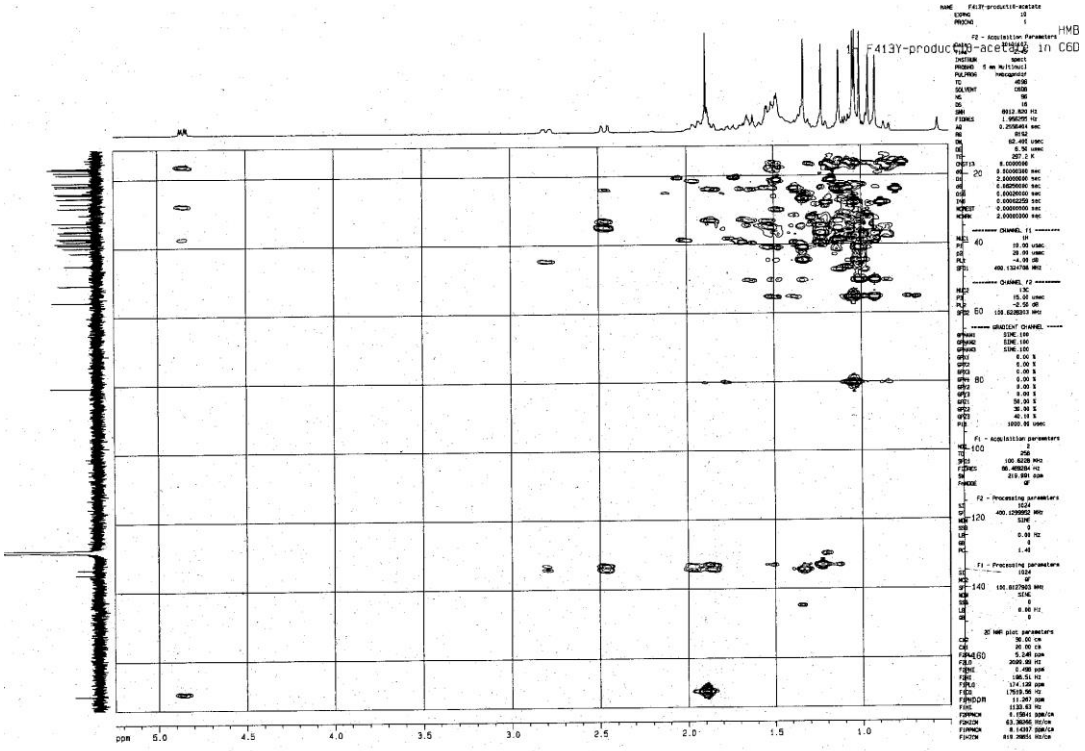

Fig. S3-10. NMR data analyses for proposing structure of **12**-Ac, optical rotation and HRMS data.

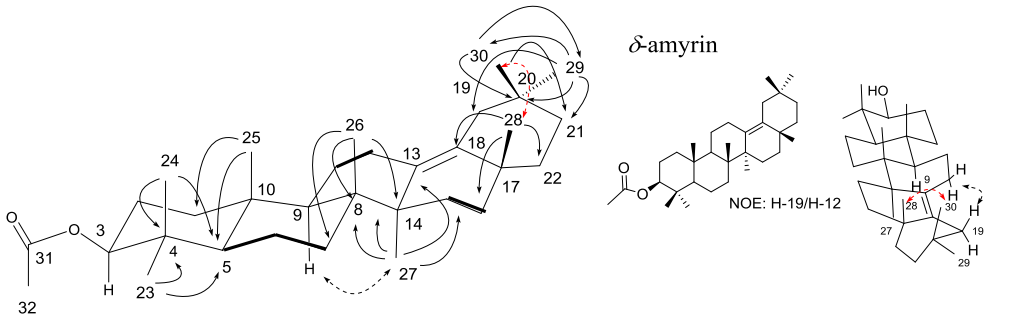

NO.	^{1}H	^{13}C	NO.	^{1}H	^{13}C	NO.	^{1}H	^{13}C	NO.	^{1}H	^{13}C
1	0.92(m);1.63(m)	38.54(t)	9	1.47 (m)	50.80(d)	17	——	34.87(s)	25	0.920(3H,s)	16.58(q)
2	1.73(m);1.88(m)	24.07(t)	10	——	37.32(s)	18	——	133.4(s)	26	1.008(3H,s)	17.90(q)
3	4.85(dd, 11.6, 4.8 Hz)	80.53 (d)	11	1.31(m);1.47(m)	22.00(t)	19	1.84 (m);2.46 (bd, J=15.6 Hz)	39.04 (t)	27	1.328(3H,s)	21.63 (q)
4	——	37.95(s)	12	1.95(m);2.78(m)	25.36(t)	20	——	33.45(s)	28	1.225(3H, s)	23.83 (q)
5	0.855 (bd, J=11.6 Hz)	55.64(d)	13	——	134.9(s)	21	1.31(m);1.63(m)	35.74 (t)	29	0.959 (3H, s)	32.52(q)
6	1.35(m);1.54(m)	18.59(t)	14	——	44.96 (s)	22	1.51 (2H, m)	39.80 (t)	30	1.125(3H, s)	24.34 (q)
7	1.48(2H.m)	35.08(t)	15	1.21(m);1.90 (m)	26.92 (t)	23	1.045(3H, s)	28.18(q)	31	——	169.9(s)
8	——	41.29 (s)	16	1.51(m); 1.63(m)	37.06(t)	24	1.035(3H,s)	16.95(q)	32	1.889 (3H, s)	20.86 (q)

Fig. S4. EIMS and NMR spectra of product **15** acetate.

Fig. S4-1. EIMS spectrum of **15**-Ac.

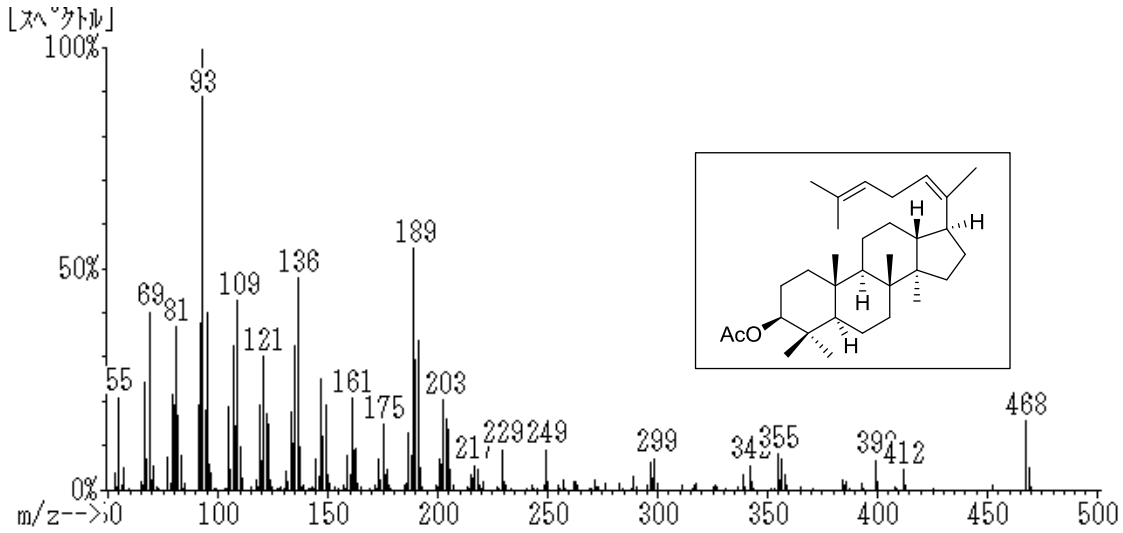

Fig. S4-2. ^{1}H-NMR spectrum of **15**-Ac in $CDCl_3$ (400 MHz).

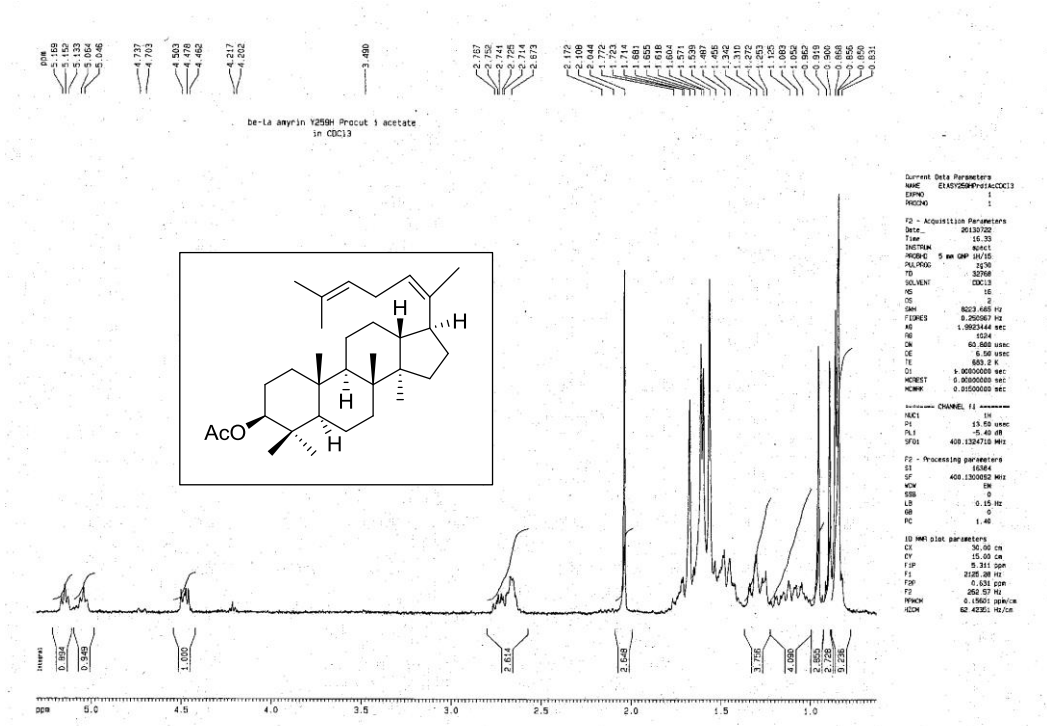

Fig. S4-3. ^{13}C NMR spectrum of **15**-Ac in $CDCl_3$ (100 MHz).

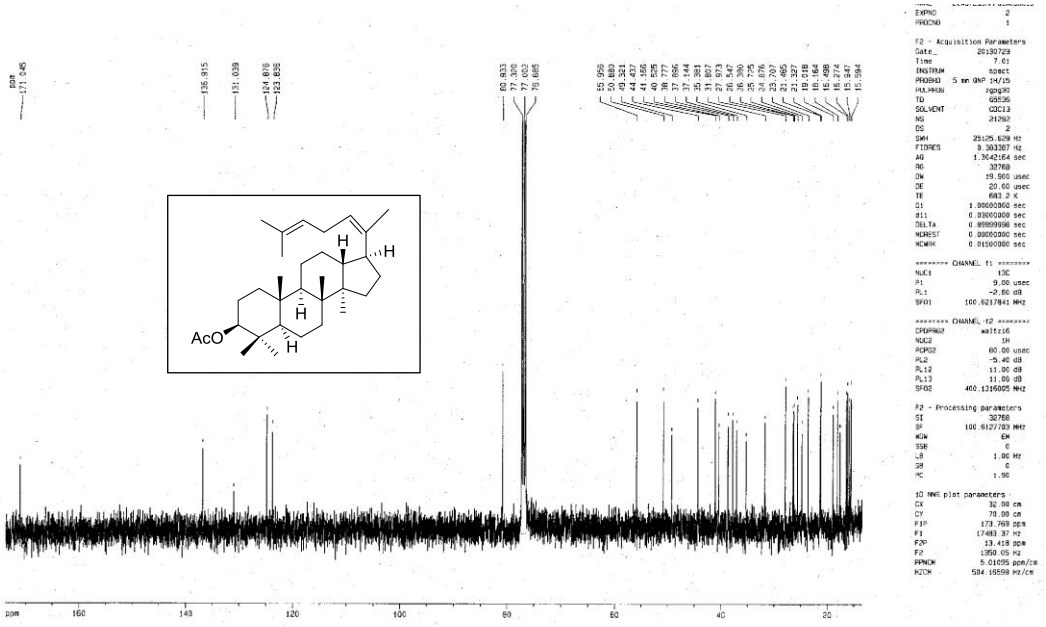

Fig. S4-4. ^{1}H-^{1}H COSY spectrum of **15**-Ac in $CDCl_3$.

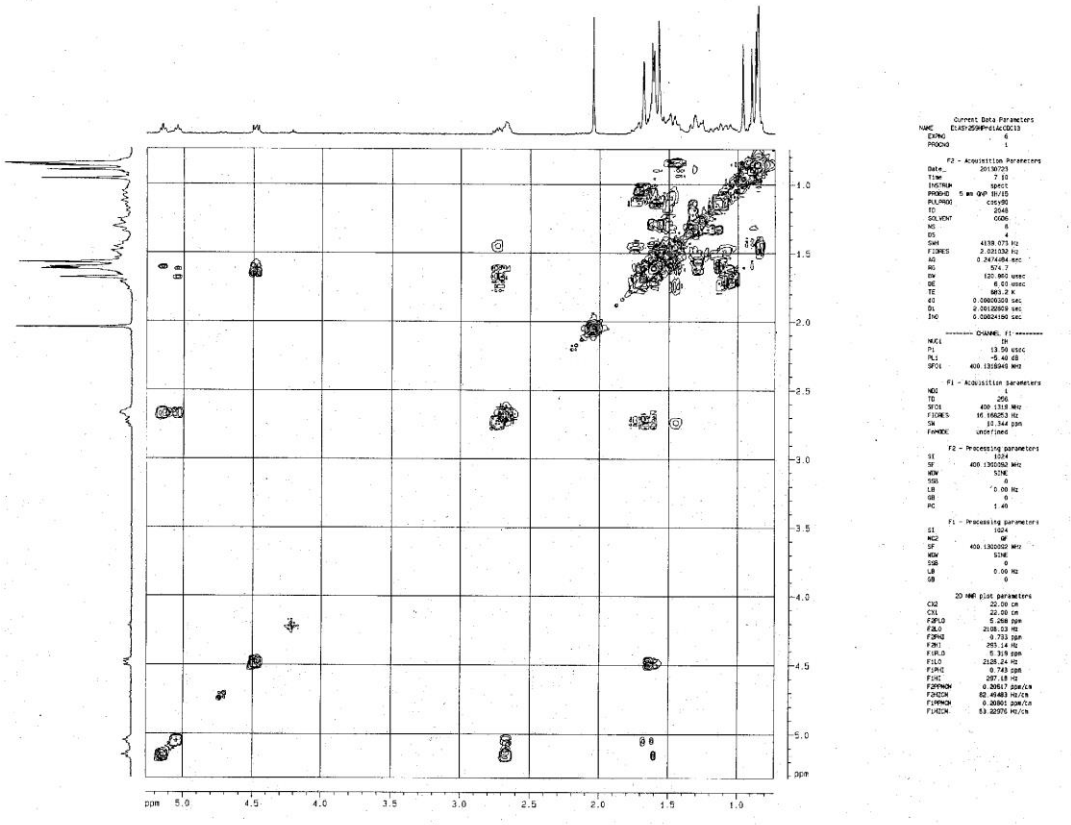

Fig. S4-5. HOHAHA spectrum of **15**-Ac in $CDCl_3$.

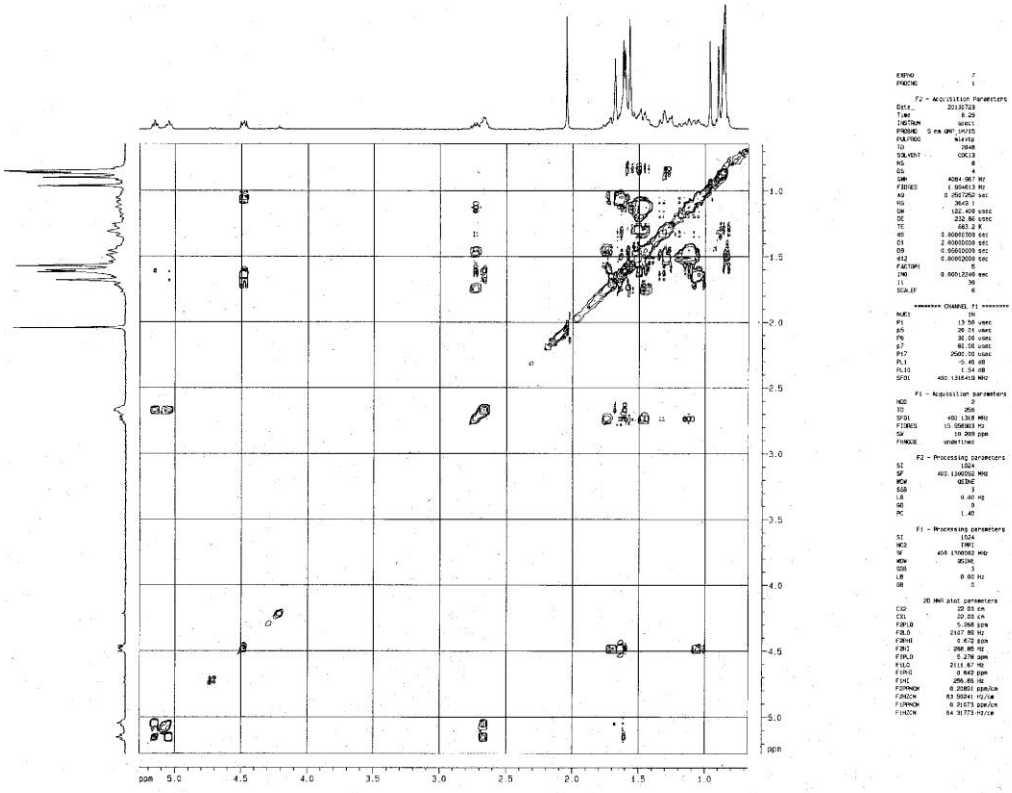

Fig. S4-6. NOESY spectrum of **15**-Ac in $CDCl_3$.

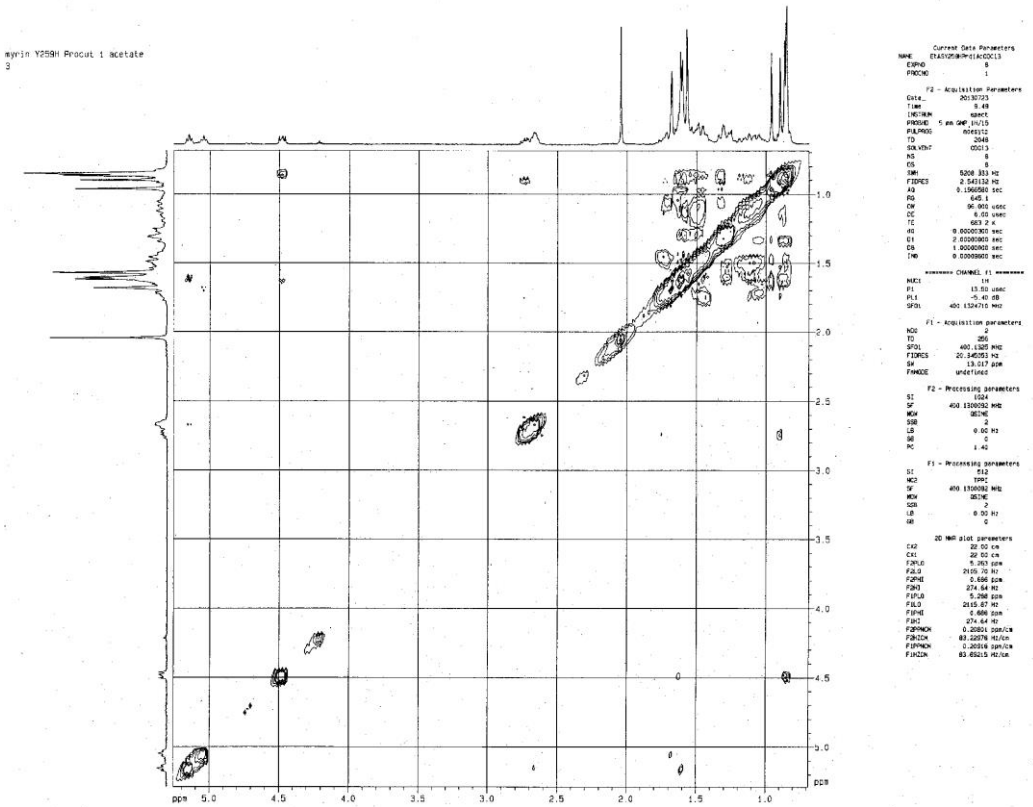

Fig. S4-7. HSQC spectrum of **15**-Ac in $CDCl_3$.

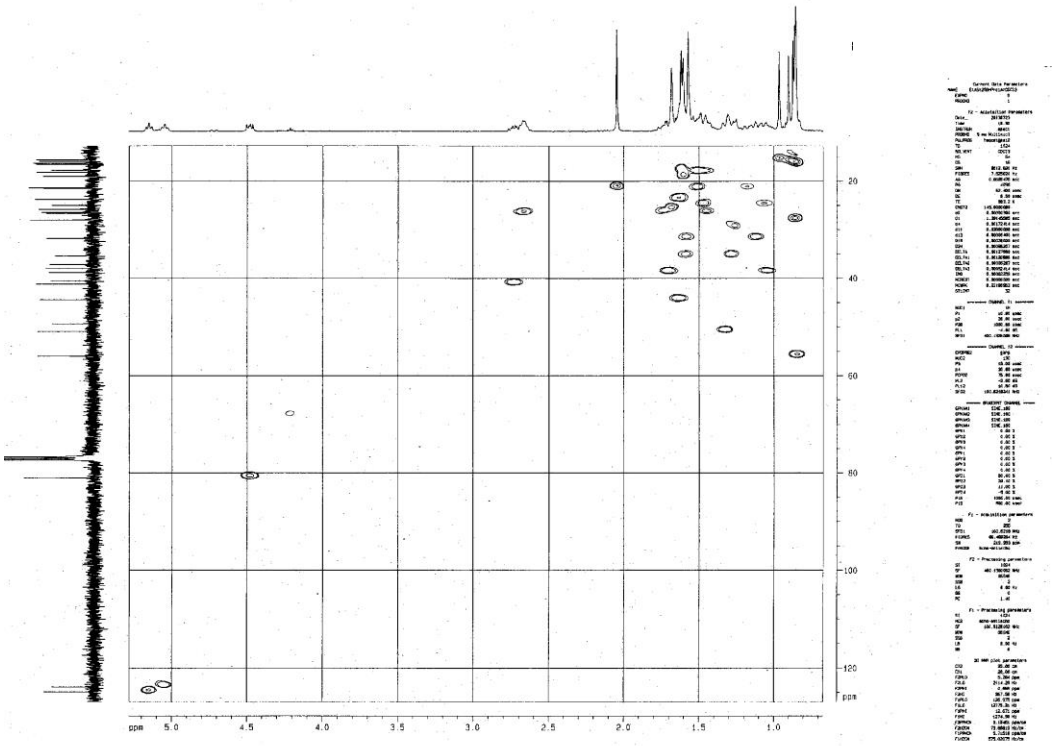

Fig. S4-8. HMBC spectrum of **15**-Ac in $CDCl_3$.

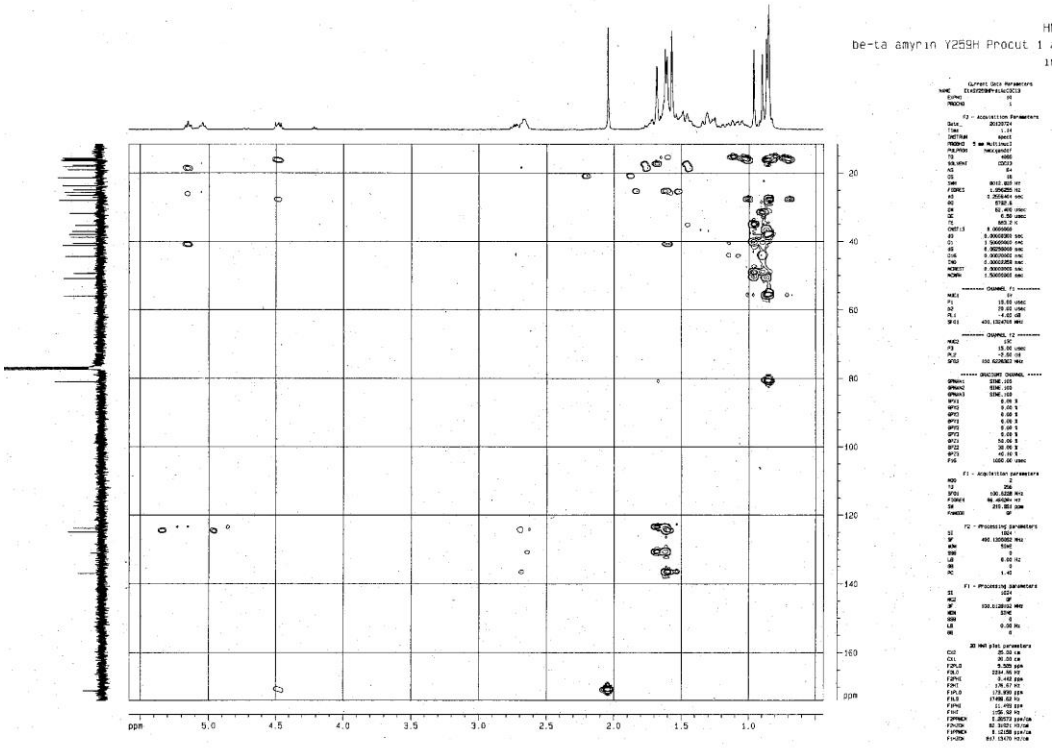

Fig. S4-9. NMR data analyses for proposing structure of **15**-Ac, optical rotation and HRMS data.

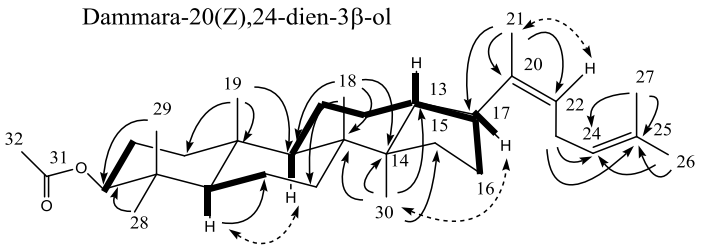

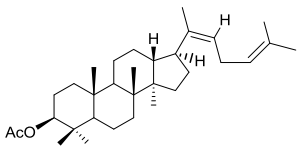

400 MHz in $CDCl_3$
the solvent peak ^1H: 7.26 ppm; ^{13}C:77.0 ppm

HREIMS
M^+: Obss. 468.39780; Calcd. 468.39673
$[\alpha]_D^{20}$= +63.3 (*c*=0.035, $CHCl_3$)

NO.	^1H	^{13}C	NO.	^1H	^{13}C	NO.	^1H	^{13}C	NO.	^1H	^{13}C
1	1.05 (m);1.71(m)	38.77	9	1.34 (m)	50.88	17	2.73 (1H, m)	41.17	25	—	131.0
2	1.64 (2H, m)	23.71	10	—	37.14	18	0.962 (3H, s)	15.59	26	1.681 (3H,s)	25.72
3	4.48 (dd, J=10.3, 6.4 Hz)	80.93	11	1.17 (m); 1.52(m)	21.47	19	0.868 (3H, s)	16.27	27	1.618 (3H, s)	17.71
4	—	37.90	12	1.06 (m);1.47(m)	24.88	20	—	136.9	28	0.856 (3H, s)	27.97
5	0.84 (1H, m)	55.96	13	1.63(1H, m)	44.44	21	1.604 (3H,s)	19.02	29	0.850 (3H, s)	16.50
6	1.50 (2H, m)	18.16	14	—	49.32	22	5.15 (t, J=7.2 Hz)	124.8	30	0.900 (3H,s)	15.95
7	1.28(m); 1.58(m)	35.38	15	1.12(m); 1.58(m)	31.81	23	2.66 (2H, m)	26.38	31	—	171.0
8	—	40.53	16	1.45 (m);1.73 (m)	26.55	24	5.06 (t, J=7.2 Hz)	123.8	32	2.044(3H, s)	21.33

Fig. S5. EIMS and NMR spectra (400 MHz, C_6D_6) of product **17**-acetate

Fig. S5-1. EIMS spectrum of product **17**-Ac.

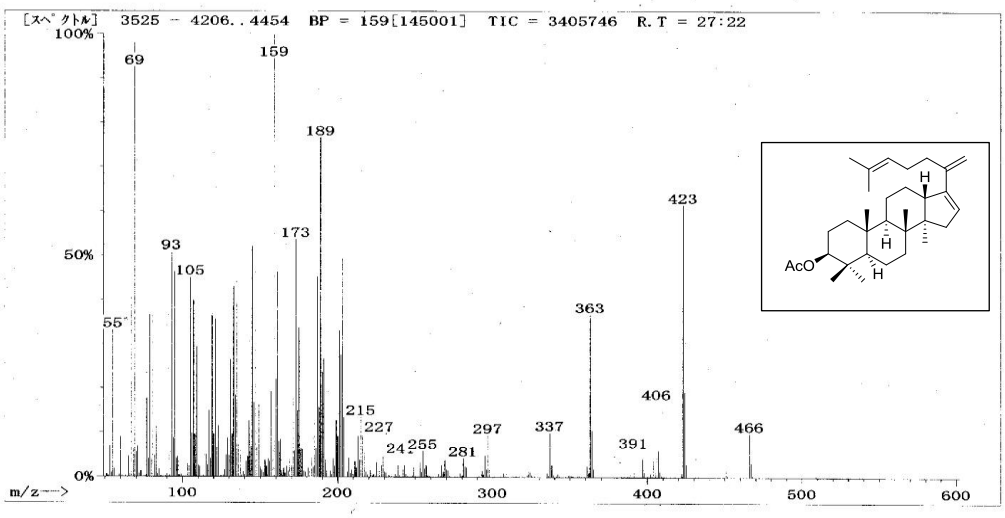

Fig. S5-2. ^{1}H-NMR spectrum of product **17**-Ac (400 MHz, C_6D_6).

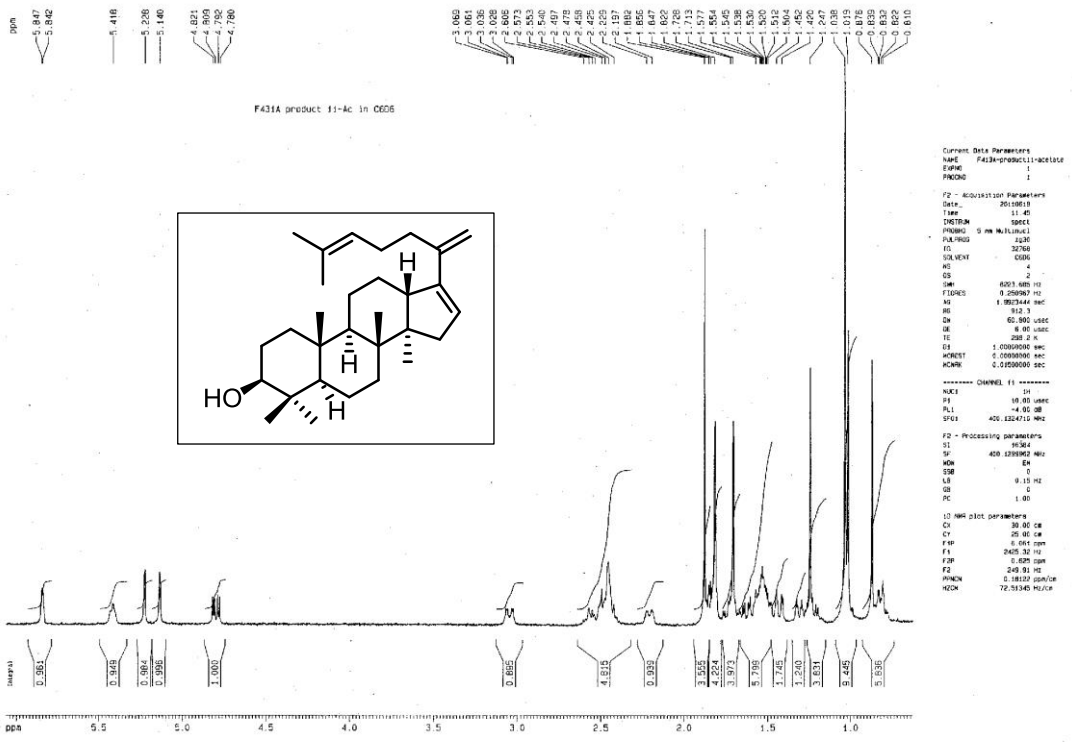

Fig. S5-3. ^{13}C-NMR spectrum of product **17**-Ac (100 MHz, C_6D_6).

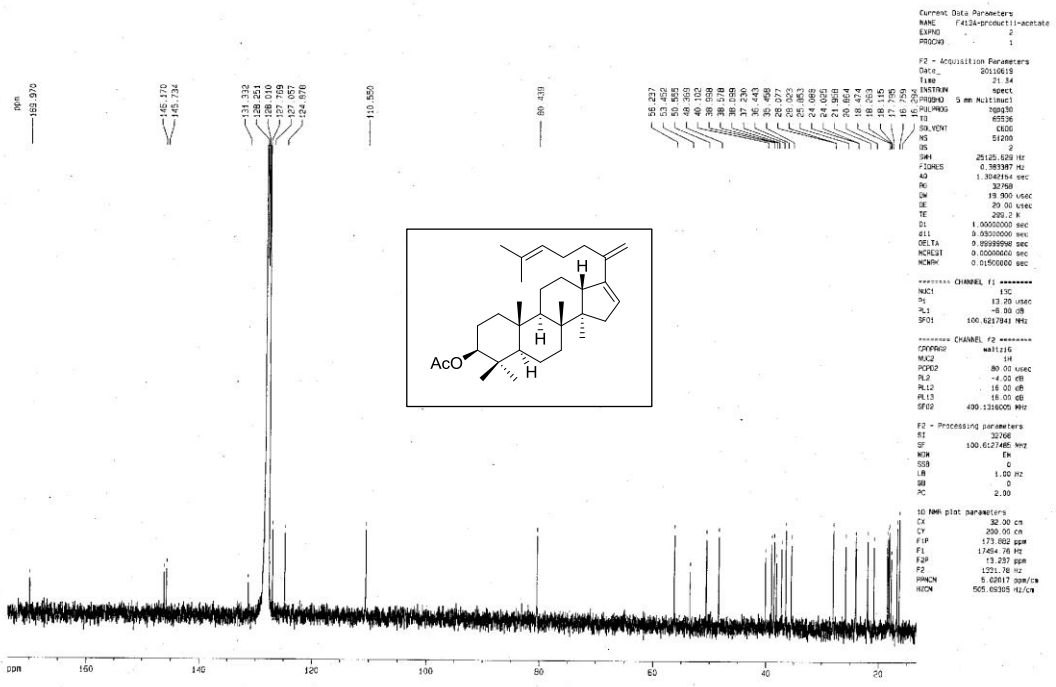

Fig. S5-4. ^{1}H-^{1}H COSY spectrum of product **17**-Ac.

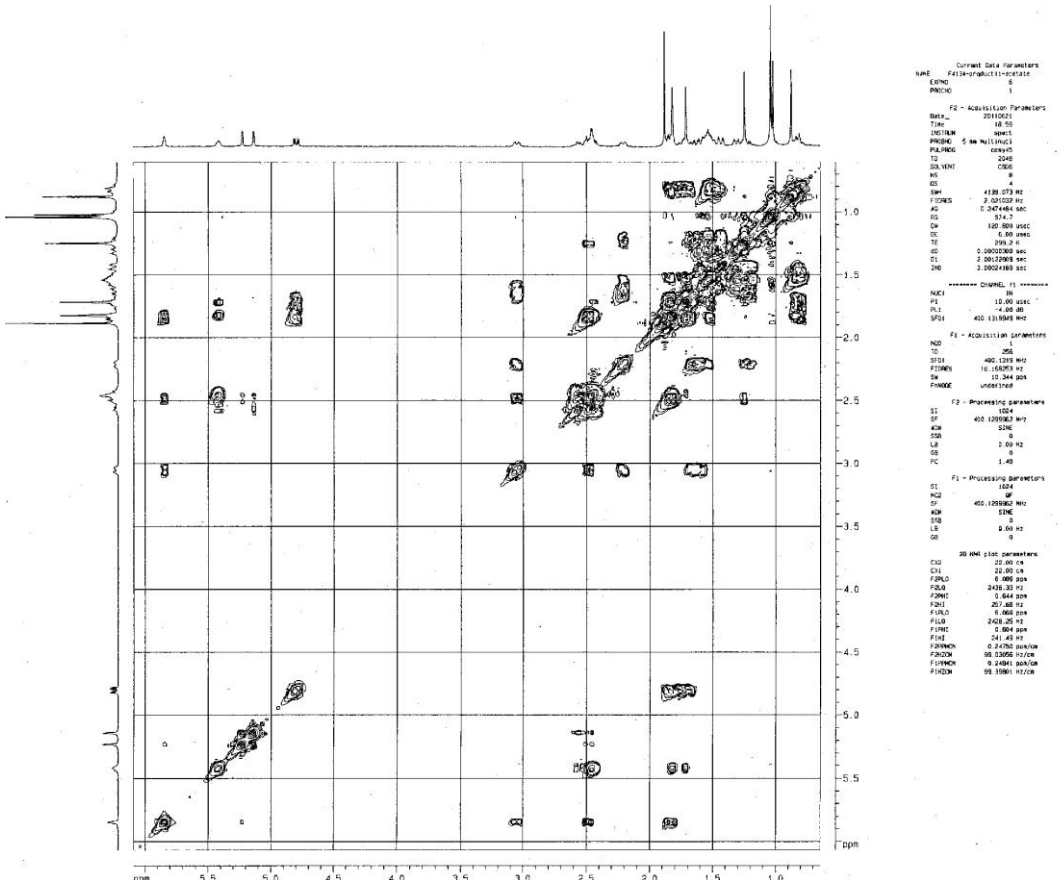

Fig. S5-5. HOHAHA spectrum of product **17**-Ac.

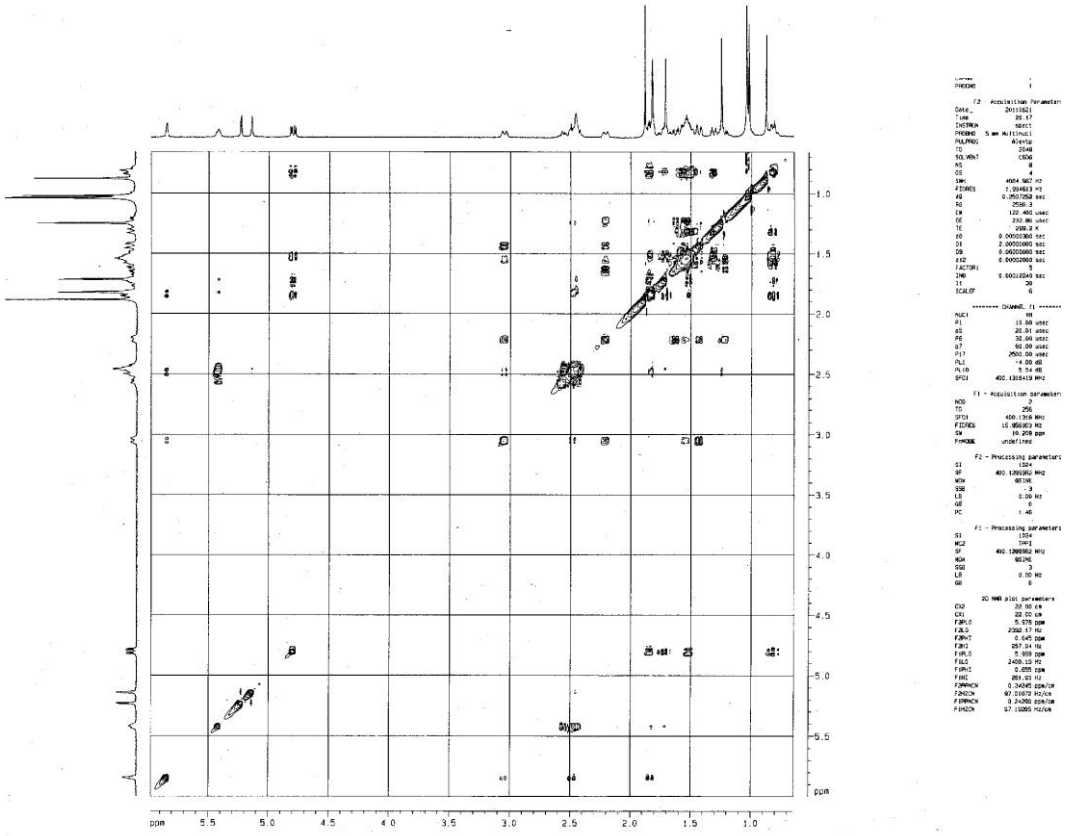

Fig. S5-6. NOESY spectrum of product **17**-Ac.

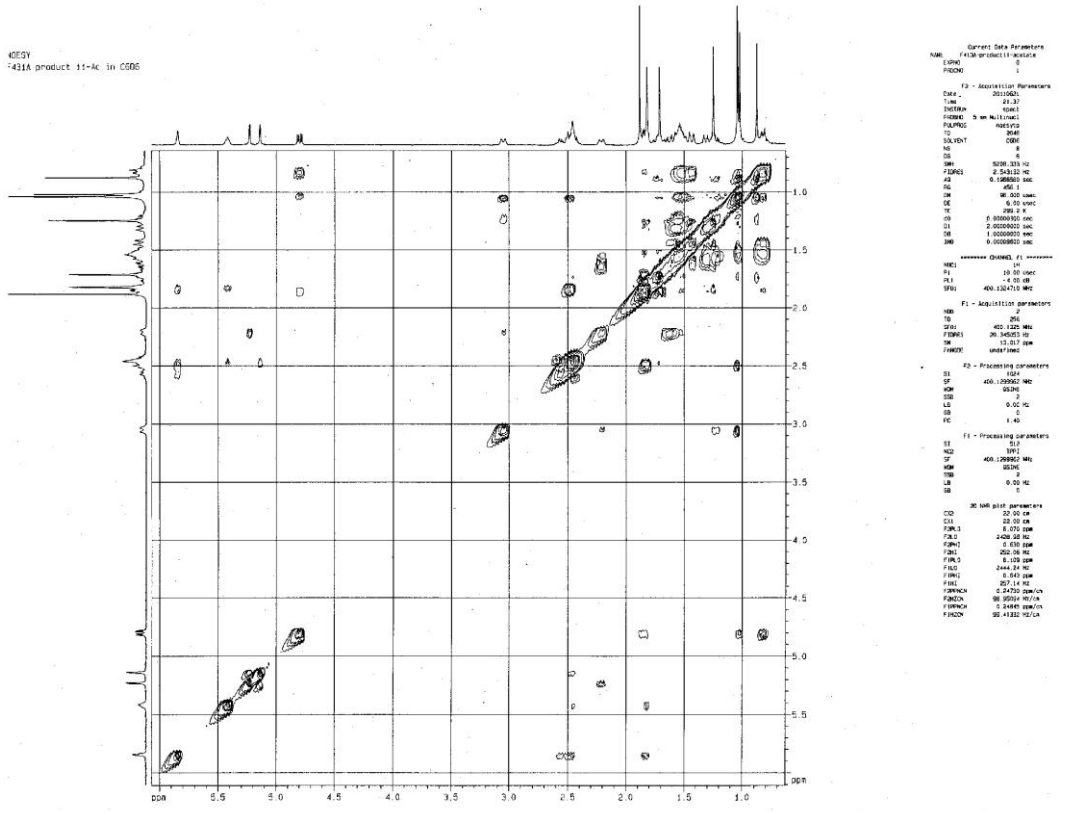

Fig. S5-7. HSQC spectrum of product **17**-Ac.

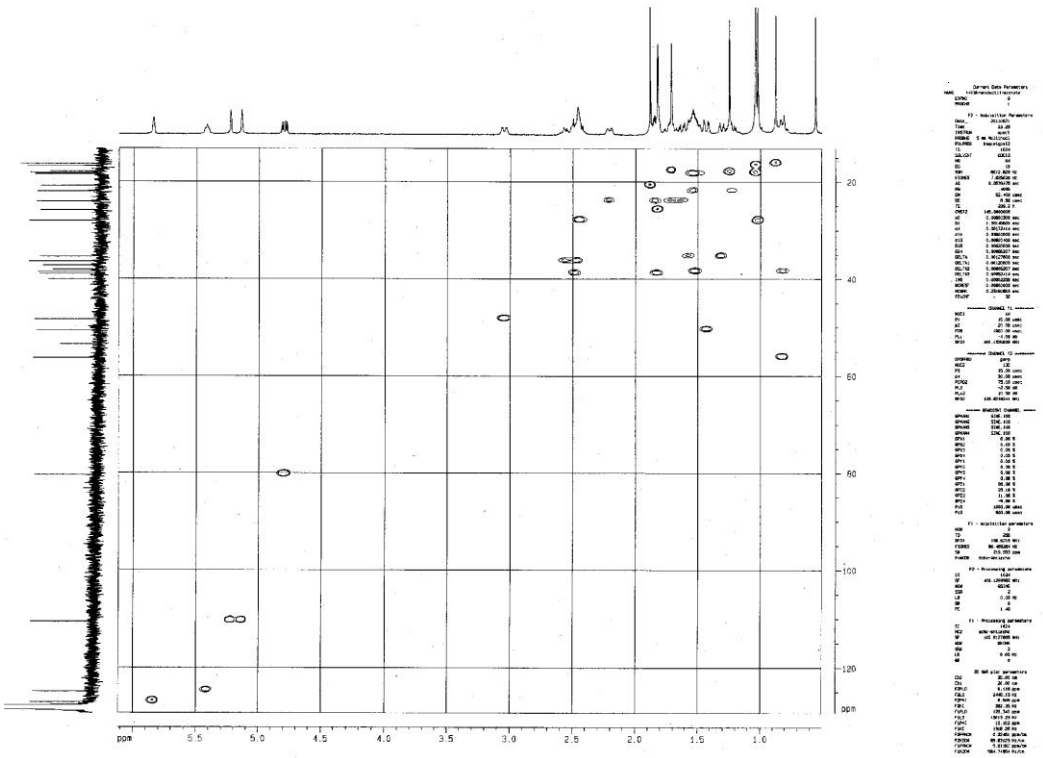

Fig. S5-8. HMBC spectrum of product **17**-Ac.

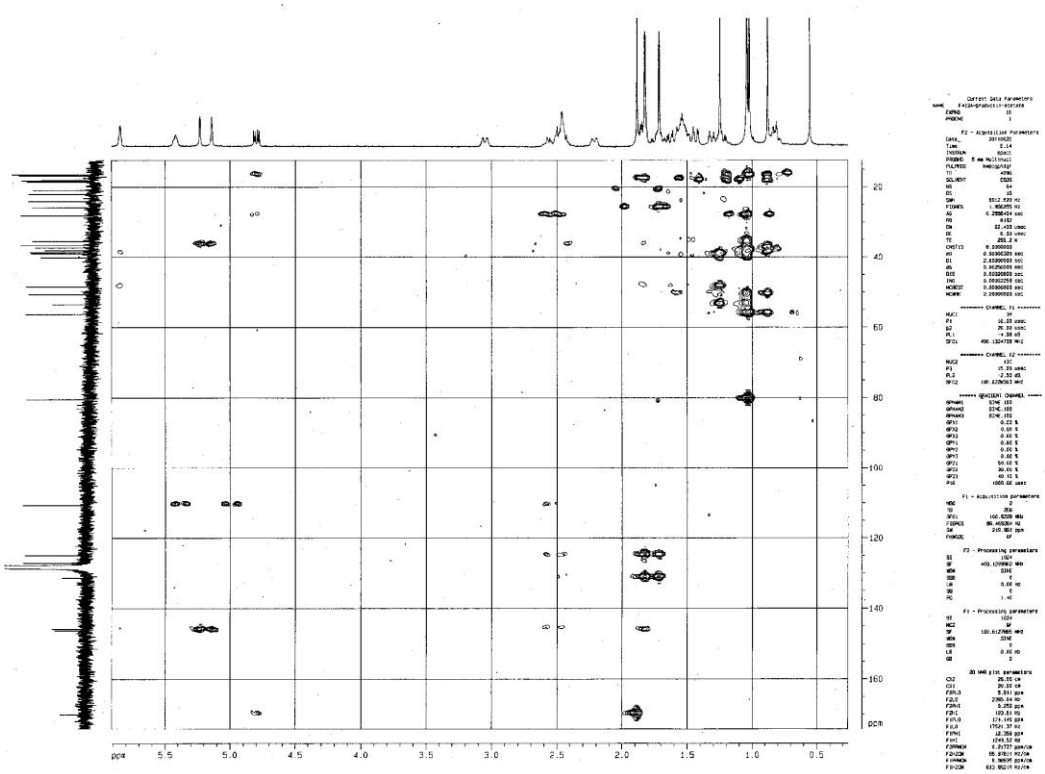

Fig. S5-9. NMR data analyses for proposing structure of **17**-Ac and HREIMS data. Reliable optical rotation was not obtained due to the sample loss during isolation and the instrumental analyses.

Product **17** acetate in C_6D_6

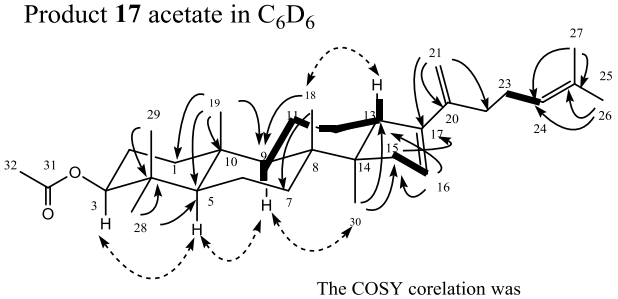

The COSY corelation was observed between H-16 and H-13.

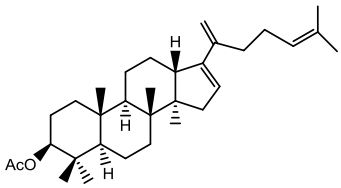

HREIMS M+: Obsd. 466.38168
Calcd. 466.38108

400 MHz in C_6D_6
the solvent peak ^1H: 7.28 ppm; ^{13}C:128.0 ppm

NOE: ◄- - - -► COSY: ▬▬ HMBC: ⟶

NO.	^1H	^{13}C	NO.	^1H	^{13}C	NO.	^1H	^{13}C	NO.	^1H	^{13}C
1	0.82 (m);1.52 (m)	38.58	9	1.43 (bd, 12.0 Hz)	50.56	17	—	146.2	25	—	131.3
2	1.71 (m); 1.84(m)	24.09 *a*	10	—	37.23	18	1.038 (3H, s)	18.26 *b*	26	1.822 (3H, s)	25.85
3	4.80 (dd, J=11.6, 4.8 Hz)	80.44	11	1.22 (m); 1.56(m)	21.96	19	0.876 (3H, s)	16.29	27	1.713 (3H,s)	17.80
4	—	38.09	12	1.63 (m);2.21 (bd, J=12.5 Hz)	24.03 *a*	20	—	145.7	28	1.019 (3H, s)	28.08
5	0.83 (m)	56.24	13	3.05 (1H,dd, J=13.0, 3.2 Hz)	48.37	21	5.23 (s); 5.14 (s)	110.5	29	1.038 (3H, s)	16.76 *b*
6	1.46 (m); 1.56(m)	18.47	14	—	53.45	22	2.47 (m); 2.57(m)	35.44	30	1.247 (3H,s)	16.12
7	1.31(bd, J=12.5Hz); 1.58(m)	35.46	15	1.84 (m); 2.49 (m)	39.00	23	2.45 (2H, m)	28.02	31	—	170.0
8	—	40.10	16	5.84 (bs)	127.1	24	5.42 (Very broad s)	124.9	32	1.882 (3H, s)	20.86

a and *b*: The assignments are exchangeable between the same letters.

Fig. S6. GCMS spectrum of the acetate of the hexane-extract obtained from the Y259H mutant. **19** acetate. The EIMS of **19** acetate was almost identical to that of dammara-(*E*)-20(22),(*E*)24(25)dien-3β-ol acetate that was isolated from F728H mutant (Ito, R.; Hashimoto I.; Masukawa Y.; Hoshino, T. *Chem.-Eur. J.* **2013**, *19*, 17150-17158, see Supporting Information, Fig. S36, EIMS) and is quite similar as that of EIMS of **15**-acetate.

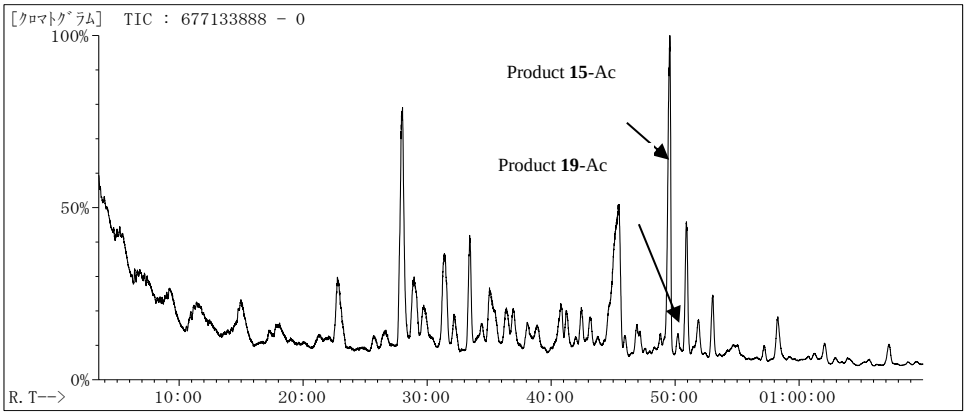

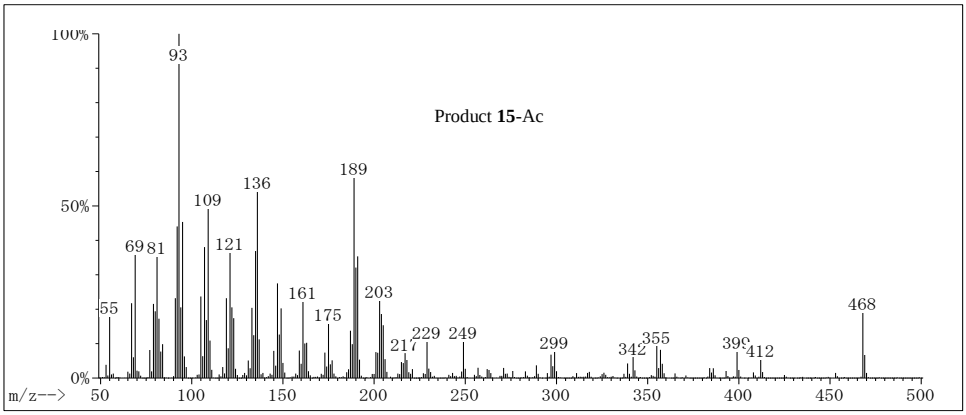

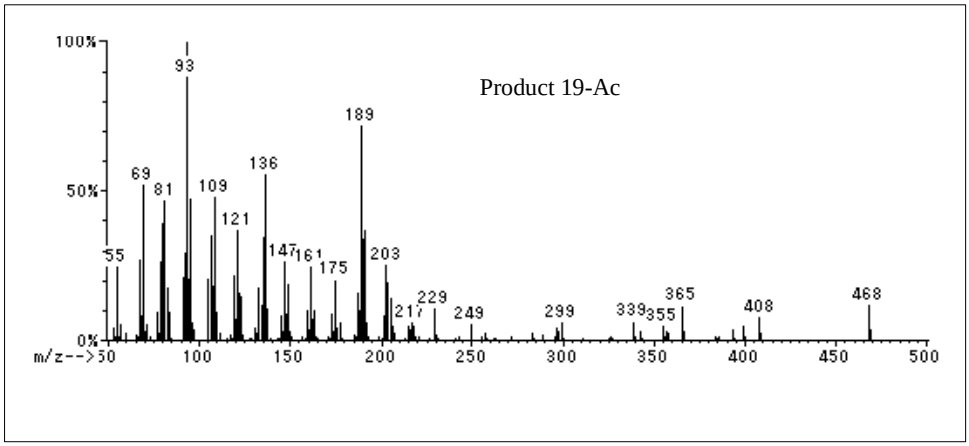

Fig. S7.1. Homology modeling of β-amyrin synthase prepared with Pymol (http://www.pymol.org). This model was constructed by ESyPred3D (http://www.unamur.be/sciences/ biologie/urbm/ bioinfo/esypred/), based on on the X-ray crystal structure of human lanosterol cyclase (pdb ID: 1w6k, *Nature* **432**, 118-122, 2004). Lambert C, Leonard N, De Bolle X & Depiereux E (2002) ESyPred3D: Prediction of proteins 3D structures *Bioinformatics*. **18**, 1250-1256.

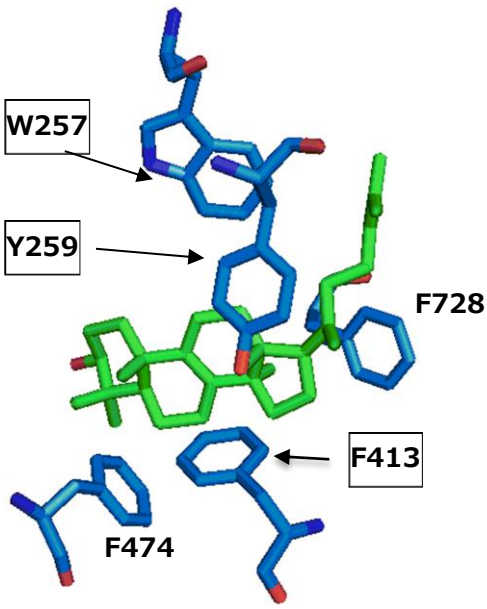

Lanosterol molecule is shown with green color. We have reported the detailed functional analysis of F728 in the previous paper (R. Ito, I. Hashimoto, Y. Masukawa and T. Hoshino, *Chem. Eur. J.* **2013**, *19*, 17150-17158). The site-directed mutagenesis experiments have demonstrated that the function of cation/π interaction was assigned to the F728 residue. On the other hand, the steric bulk at 474 position is critical to the accurate folding of oxidosqualene to complete the polycyclization reaction (Ito, R.; Masukawa, Y.; Nakada, C.; Amari, K.; Nakano, C.; Hoshino, T. *Org. Biomol. Chem*. **2014**, *12,* 3836-3846). By the mutagenesis experiments, we found that $D^{485}C^{486}TA$ motif triggers the polycyclization reaction and the C564 is involved in hydrogen bond formation with the carboxyl residue of D485, resulting in enhancement of the acidity (R. Ito, Y. Masukawa and T. Hoshino, *FEBS J.*, **2013**;*280*:1267-1280). F474 is situated in the vicinity to B-ring formation site. F413 residue is located in approximate to the C/D ring. Y259 and W257 that correspond to Y261and to W259, respectively, of *P. ginseng* PNY β-amyrin synthase, are also marked in this model. It was reported that the Y261H mutant of PNY gave the teracyclic products (see the Text and the ref. T. Kushiro, M. Shibuya, K. Masuda, Y. Ebizuka, *J. Am. Chem. Soc.*, **2000**, 122, 6816-6824. The hydrogen bonding may occur between OH of the polar amino acids (Ser, Thr or Tyr mutants) and the phenolic OH of Y259, because of the proximal distance between them (see Fig. S7.2), which would have brought about the inappropriate placement of Y259, resulting in the decreased activities of the polar amino acid-substituted mutants (see Figure 3 in Text).

Fig. S7.2. Distances between OH of Y259 and OH of polar amino acids (Ser and Thr), OH of Tyr and NH or N of His, which were estimated from the modeling constructed by the methods of ESyPred3D. Lanosterol molecule is shown with green color.

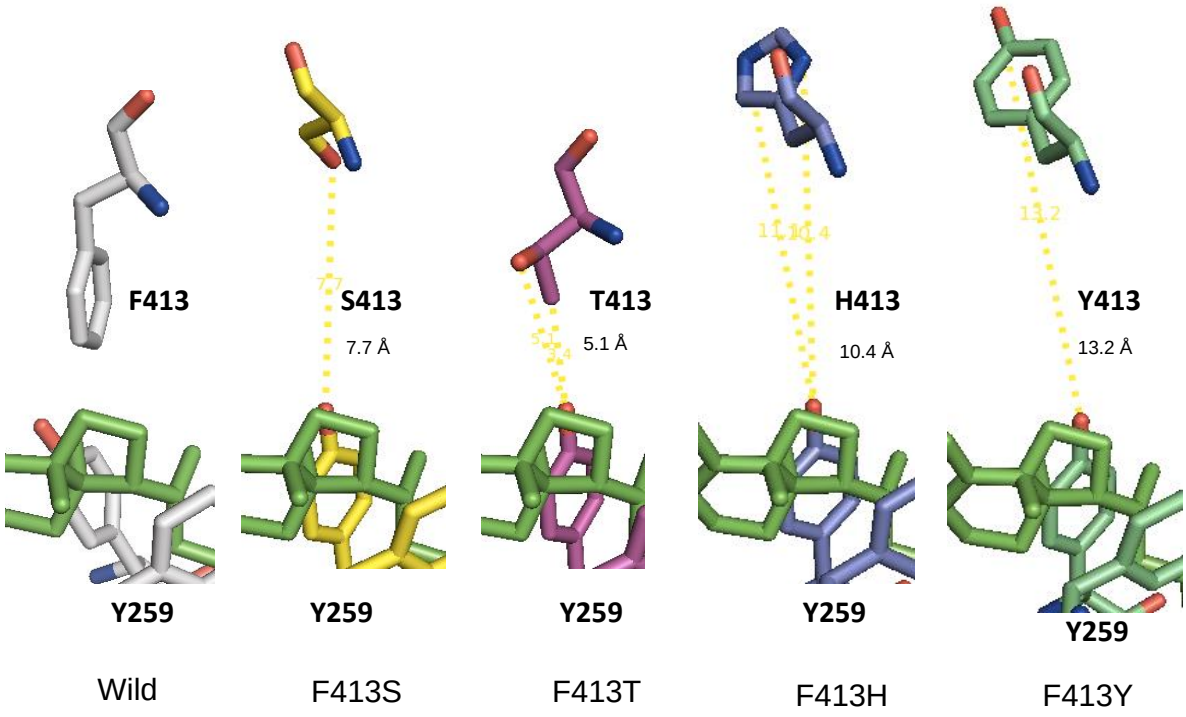

Hydrogen bonding is presumed between OH of Y259 and the polar group of Ser, Thr, His and Tyr, and water molecule(s) is also likely to intervene between the OH of Y259 and the polar groups of the substituted amino acids.

Fig. S8. GC traces of the lipophilic acetylated materials produced by various mutants targeted for F413. A 100 mL culture of each mutants were subjected to centrifugation. The cell pellets were subjected to saponification with 15% KOH/MeOH under reflux condition, followed by the extraction of the lipophilic materials with hexane extract (3 x 10 mL). The triterpene fraction including products was obtained by partial purification with a SiO_2 column to remove oxidosqualene, dioxidosqualene and nontriterpene impurities (hexane/EtOAc=100:1), followed by acetylation with Ac_2O/Py. The acetate mixture was dissolved in 1.0 mL of hexane. A 0.5 μL of the hexane was injected to the GC apparatus. The GC conditions were as follows: J & W, DB-1 capillary column (Length 30 m, I.D. 0.32 mm, Film Thickness 0.25 mm); column injection temp., 300°C; column temperature, 245-270°C (0.35 °C/min).

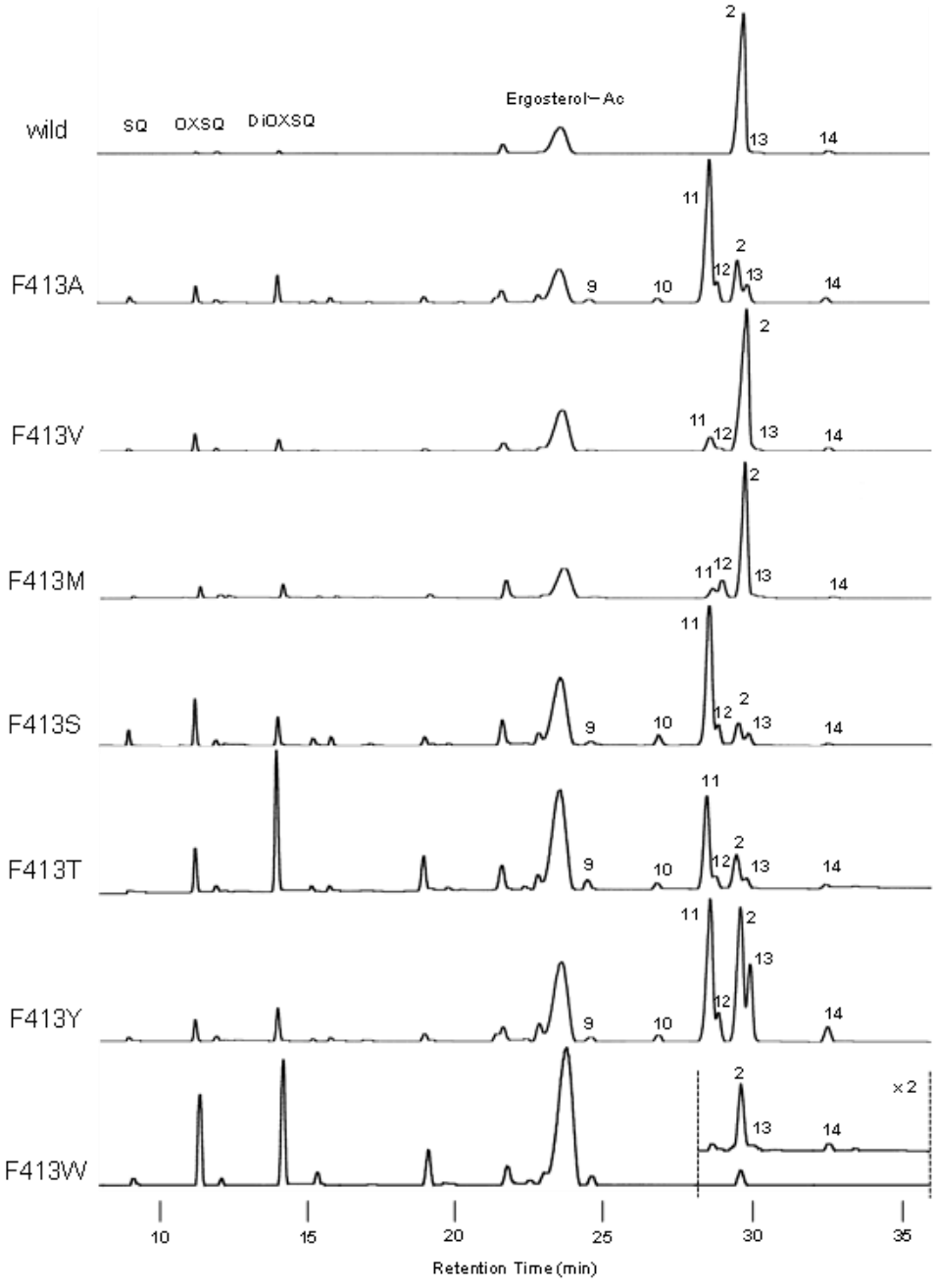

Fig. S9. Estimation of the EtAS enzymatic activities for the wild-type and the F413X mutants.

<Expression level of β–amyrin synthase (EtAS)>

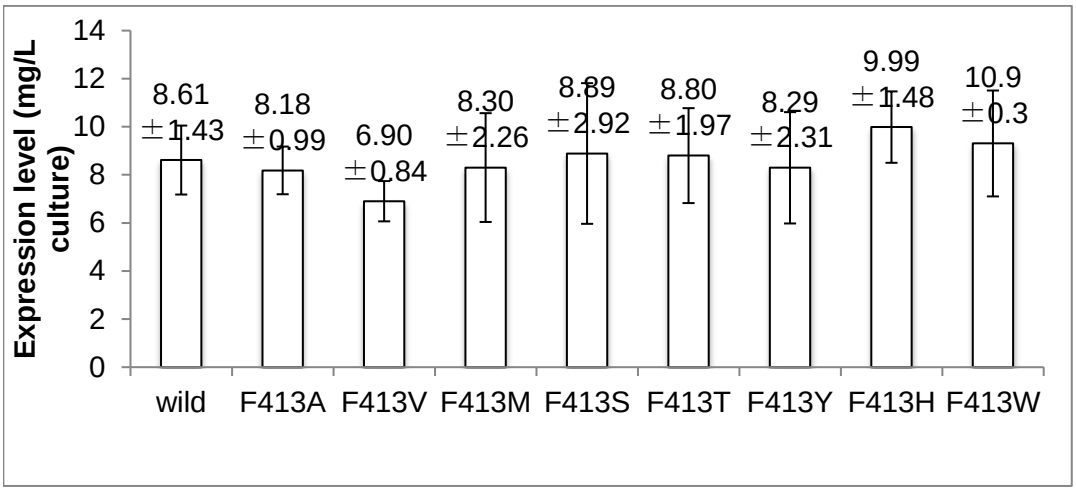

Figure S9.1. Expression level（mg/L）of the EtAS enzymes of the wild-type and the site-directed mutant. The yeast cells grown in 1L-medium were collected and the protein amounts (mg) were quantified by Western blot analysis.

＜GC analyses for the quantities of oleanane-type triterpenes＞

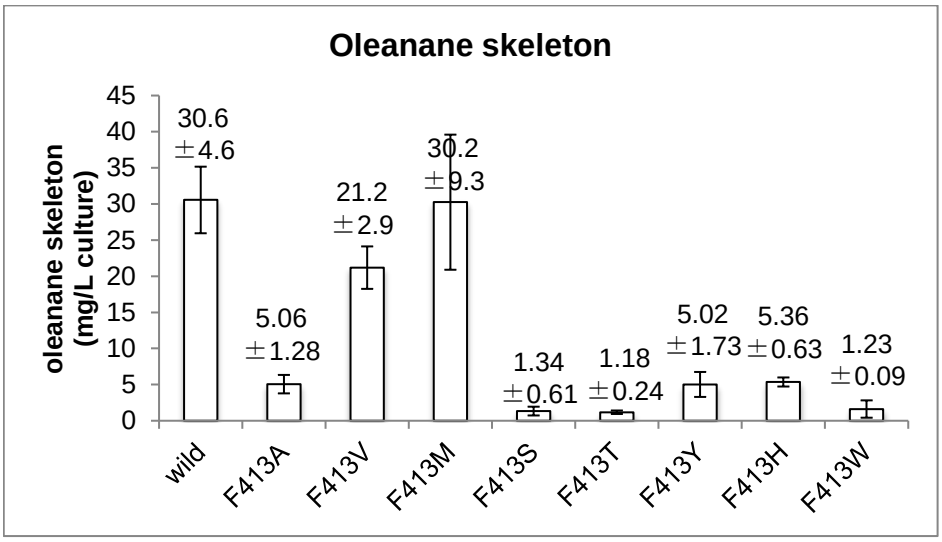

Fig. S9.2. The quantities of products **2** and **12** (oleanane skeleton) produced by 1L-culture of each of the mutant strains that were determined by GC analyses using GGOH (geranylgeraniol) as an internal standard.

＜Enzyme activities for the production of oleanane-type triterpenes＞

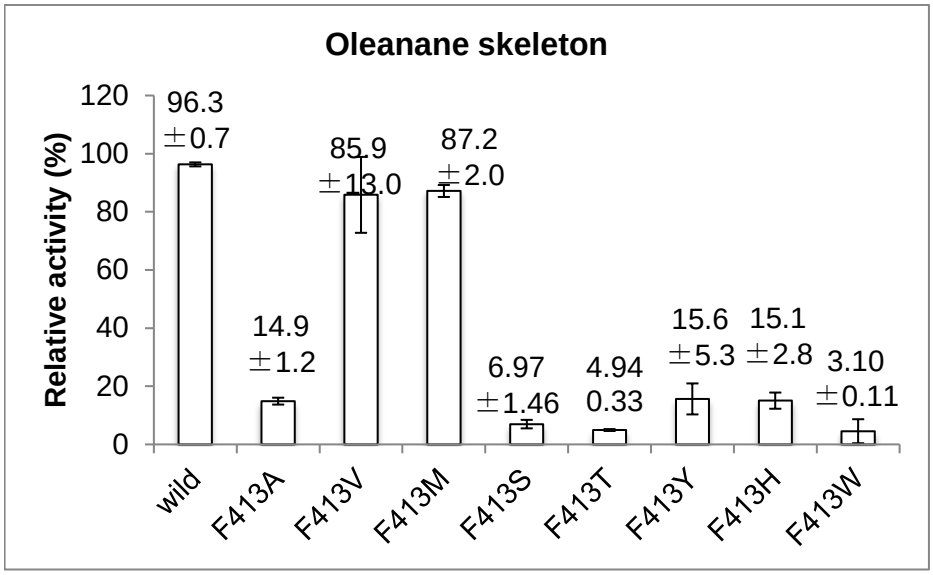

Fig. S9.3. Enzyme activities of the mutants relative to that of the wild-type for the production of oleanane skeleton. The wild-type activity (100%) indicates the sum of the relative activities shown in Figs. S9.3, Fig. S9.5 and S9.7.These enzyme activities were estimated by dividing the amounts of oleanane-type products (**2** and **12**) by the expressed quantities of EtAS enzymes. This means that the values of Fig. S9.2 were divided by those of Fig. S9.1. The wild-type did not show 100% activity, i.e., 96.3±0.7 %, because the wild-type produced the tetracycles **13** and **14** in a small amount (see Figs. S9.5 and S9.7).

< GC analyses for the quantities of Dammarane-types>

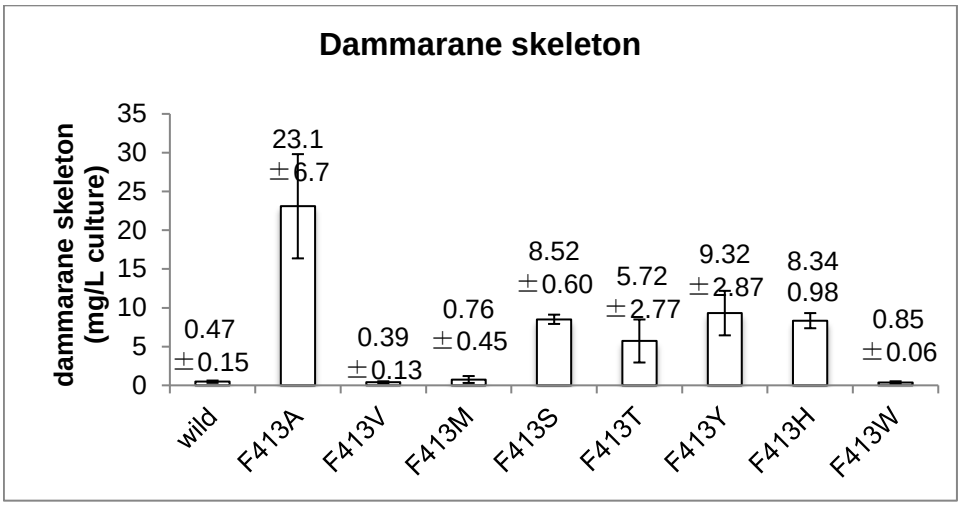

Fig. S9.4. The quantities of products **10**, **11**, **13** (dammarane skeleton) produced by 1L-culture of each of the mutant strains that were determined by GC analyses using GGOH (geranylgeraniol) as an internal standard. Product **10** is tentatively categorized as Dammarane skeleton, but not 17-epi-dammaraen skeleton. To make sense, the stereochemistry of C-20 must be determined.

< Enzyme activities for the production of Dammarane-types>

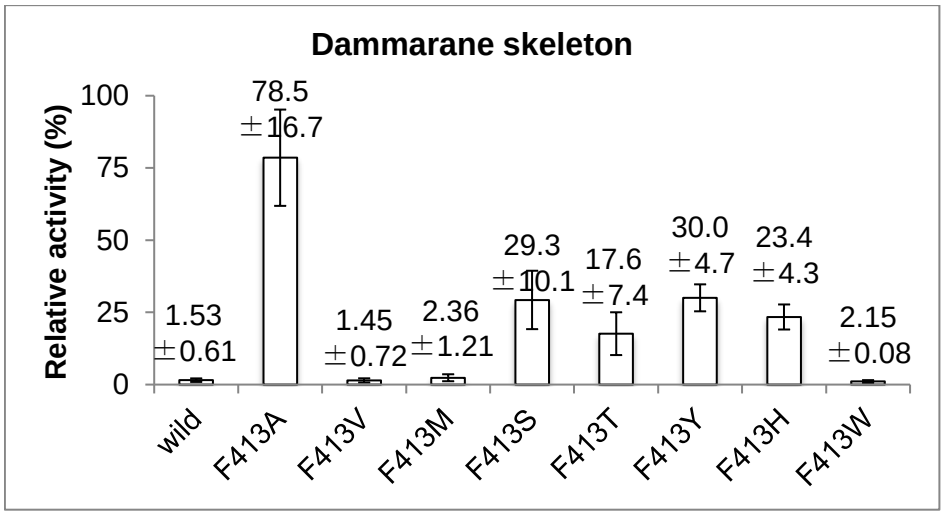

Figure S9.5. Enzyme activities of the mutants relative to that of the wild-type. These enzyme activities were estimated by dividing the amounts of dammarane-type products (**10**, **11**, **13)** by the expressed quantities of EtAS enzymes, that is, the values of Fig. S9.4 were divided by those of Fig. S9.1. The activity of the wild-type for the production of **13** and **14** was very low, i.e., 1.53±0.61%, thus, the relative activity does not correspond to 100%. The total values of Fig.S9.3 and Fig. S9.5 for the wild-type corresponds to 100%.

< GC analyses for the quantities of 17-*epi*-Dammarane-type>

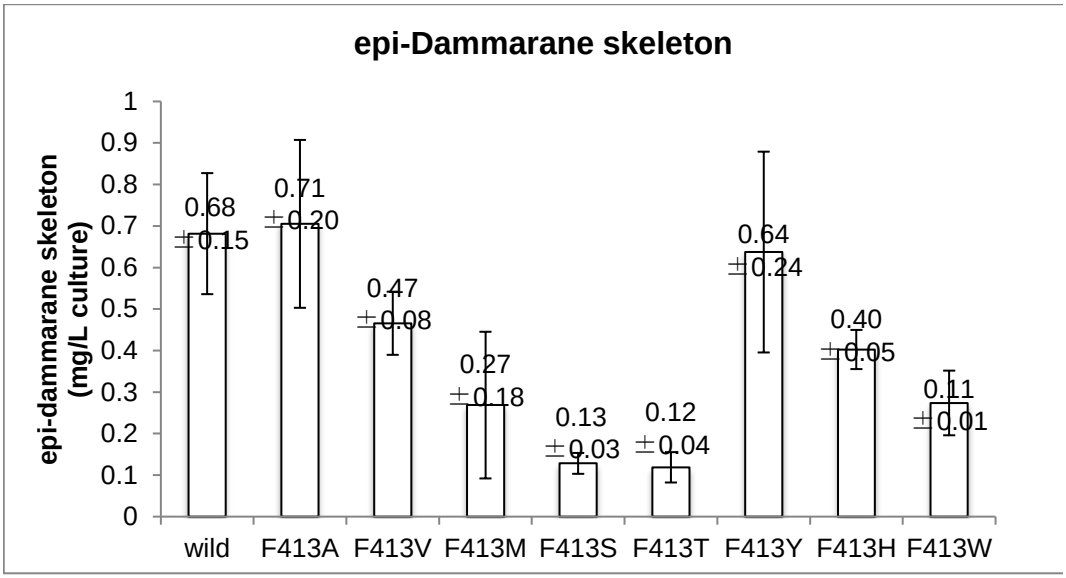

Fig. S9.6. The quantities of products **14** (17-*epi*-dammarane skeleton) produced by 1L-culture of each of the mutant strains, which were determined by GC analyses using GGOH (geranylgeraniol) as an internal standard.

< Enzyme activities for the production of 17-*epi*-Dammarane-types>

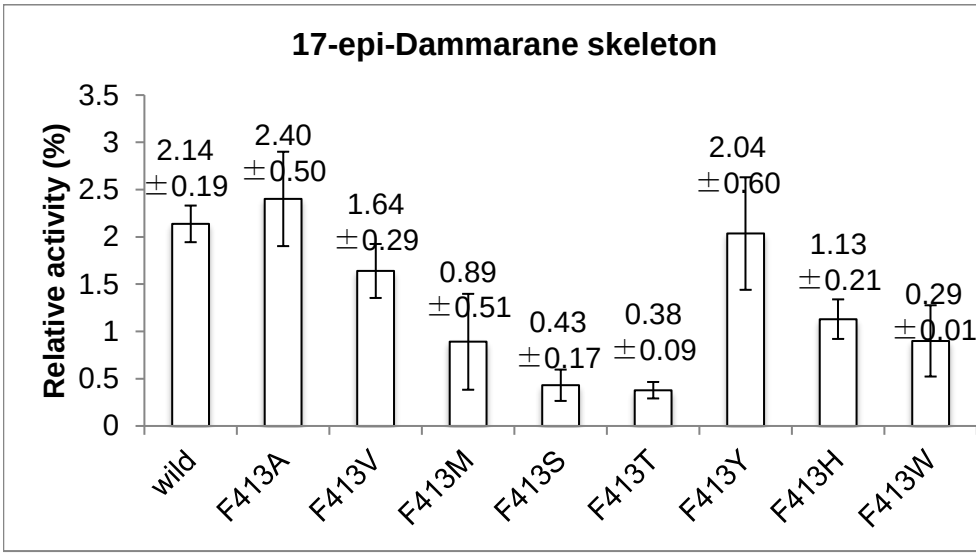

Figure S9.7. Enzyme activities of the mutants relative to that of the wild-type. These enzyme activities were estimated by dividing the amounts of 17-ep-dammarane-type product **14** by the expressed quantities of EtAS enzymes (%).

< GC analyses for the quantities of bicyclic product >

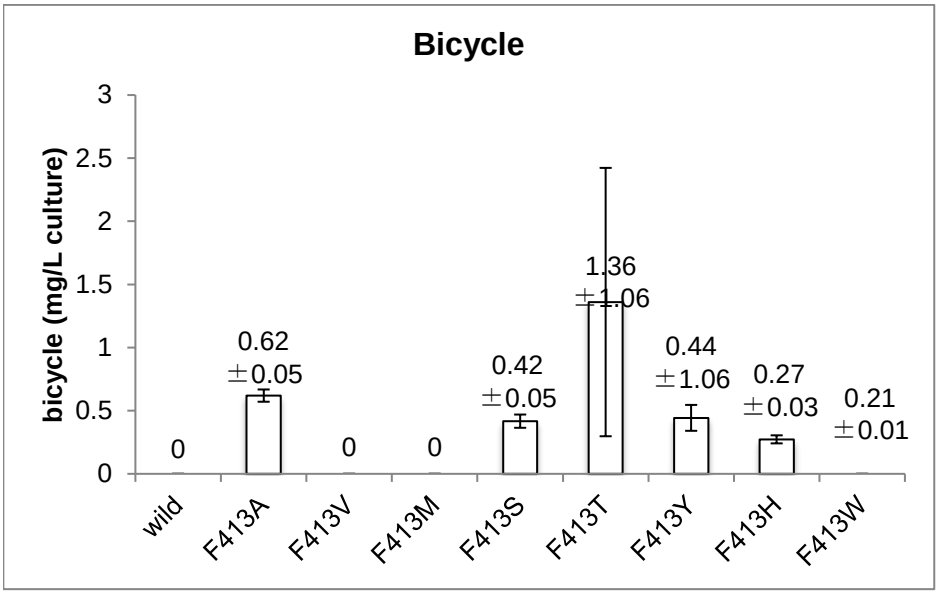

Fig. S9.8. The quantities of products **9** produced by 1L-culture of each of the mutant strains, which were determined by GC analyses using GGOH (geranylgeraniol) as an internal standard.

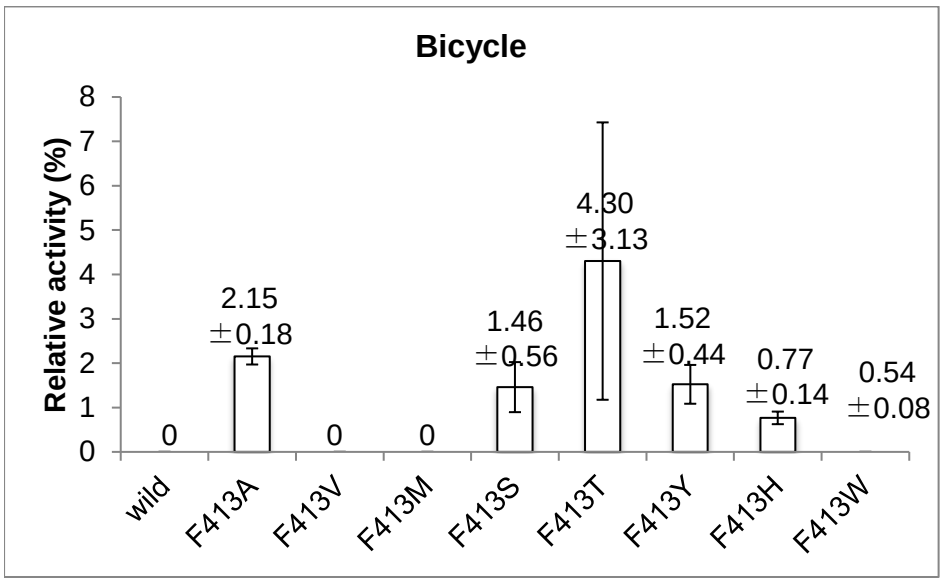

Figure S9.9. Enzyme activities of the mutants relative to that of the wild-type. These enzyme activities were estimated by dividing the amounts of bicyclic product **9** by the expressed quantities of EtAS enzymes (%).

Fig. S10. Estimation of the EtAS enzyme activities for the Y259X mutants.

<Expression level of β–amyrin synthase (EtAS)>

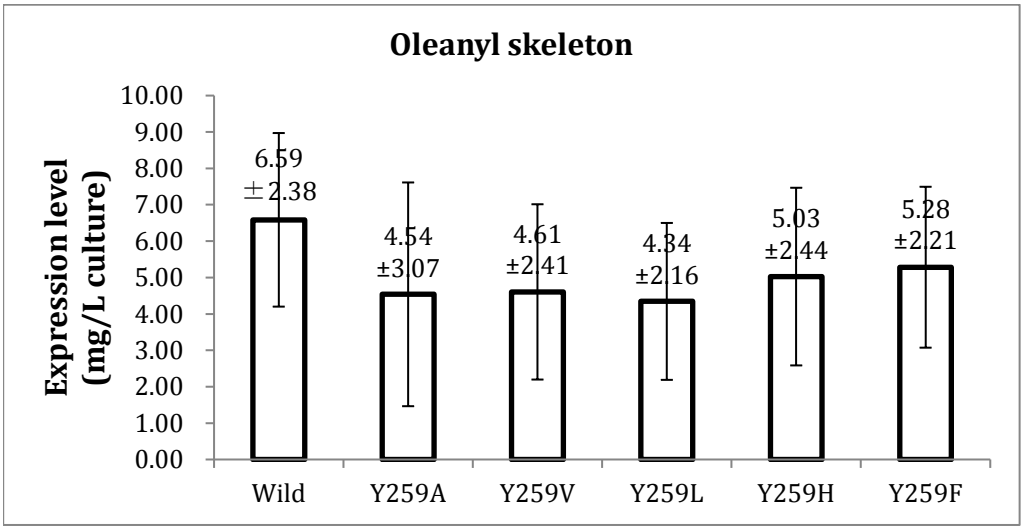

Fig. S10.1. Expression level（mg/L）of the EtAS enzymes of the wild-type and the site-directed mutant. The yeast cells grown in 1L-medium were collected and the protein amounts (mg) were quantified by Western blot analysis.

＜GC analyses for the quantities of oleanane-type triterpenes＞

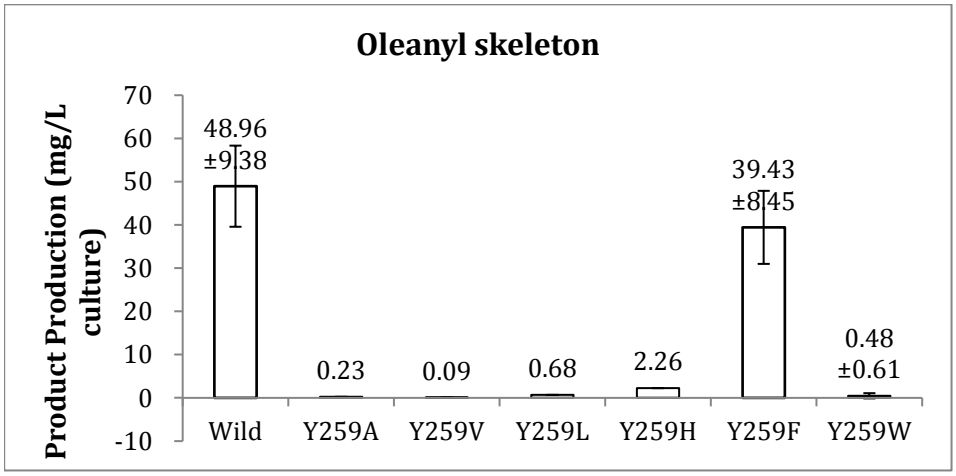

Fig. S10.2. The quantities of products **2**, **16** and **18** (oleanane skeleton) produced by 1L-culture of each of the mutant strains that were determined by GC analyses using GGOH (geranylgeraniol) as an internal standard.

＜Enzyme activities for the production of oleanane-type triterpenes＞

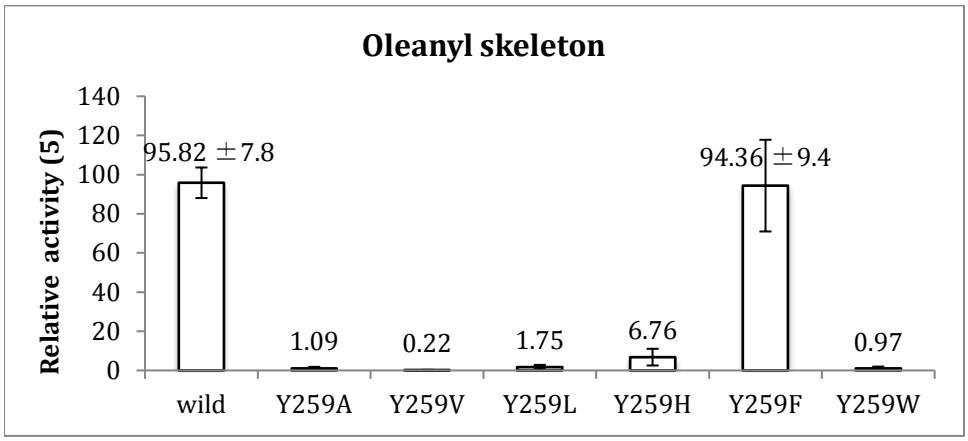

Fig. S10.3. Enzyme activities of the mutants relative to that of the wild-type for the production of oleanane skeleton. See the legend to Fig. S9.3 for the calculation method.

＜GC analyses for the quantities of lupanyl-type triterpene, lupeol＞

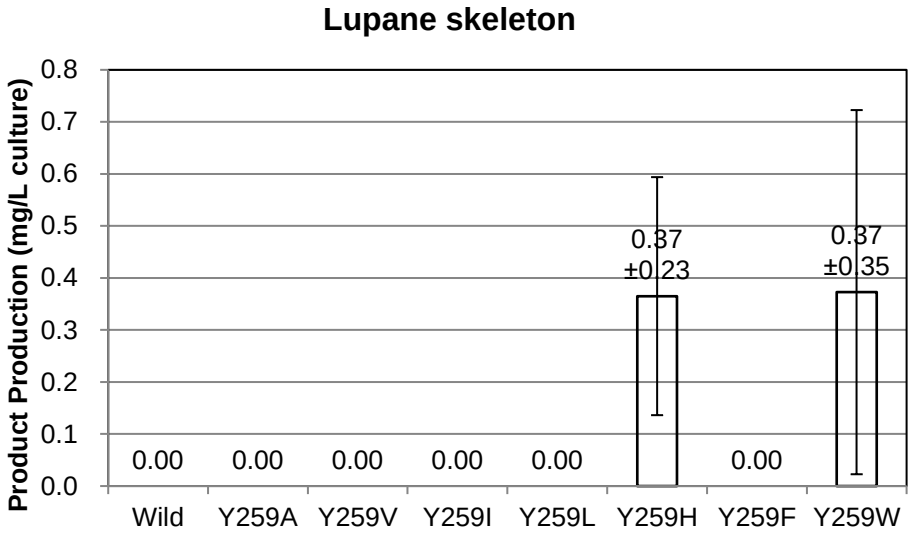

Fig. S10.4. The quantities of product **20** (lupeol, 6/6/6/6/5-fused pentacycle) produced by 1L-culture of each of the mutant strains that were determined by GC analyses using GGOH (geranylgeraniol) as an internal standard.

＜Enzyme activities for the production of lupeol＞

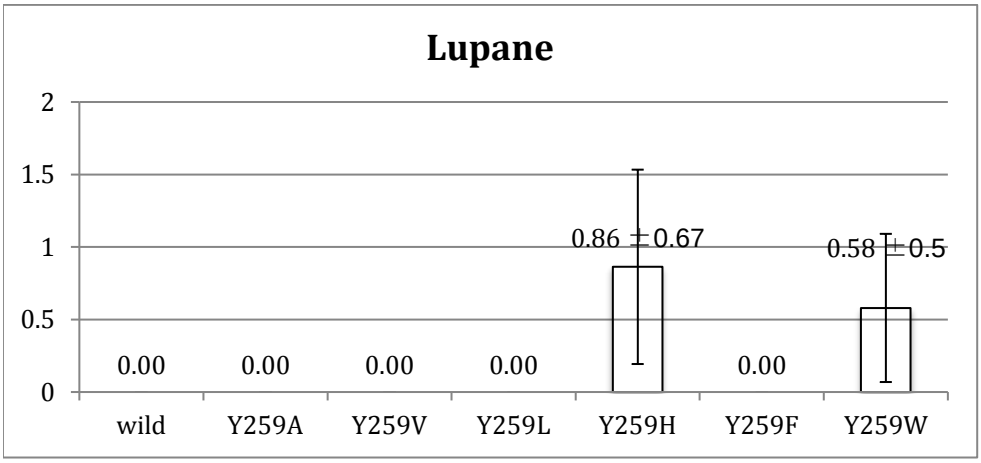

Fig. S10.5. Enzyme activities of the mutants relative to that of the wild-type. These enzyme activities were estimated by dividing the amounts of lupanyl-type product **20** by the expressed quantities of EtAS enzymes.

＜GC analyses for the quantities of tetracyclic triterpenes＞

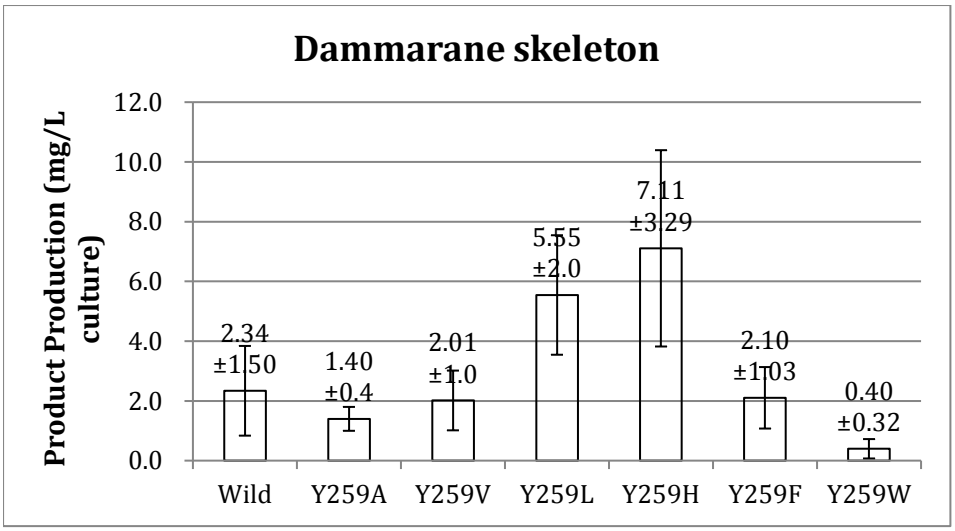

Fig. S10.6. The total quantities of products **11**, **13**, **14**, **15**, **17** and **19** produced by 1L-culture of each of the mutant strains that were determined by GC analyses using GGOH (geranylgeraniol) as an internal standard.

＜Enzyme activities for the production of dammarenyl skeleton＞

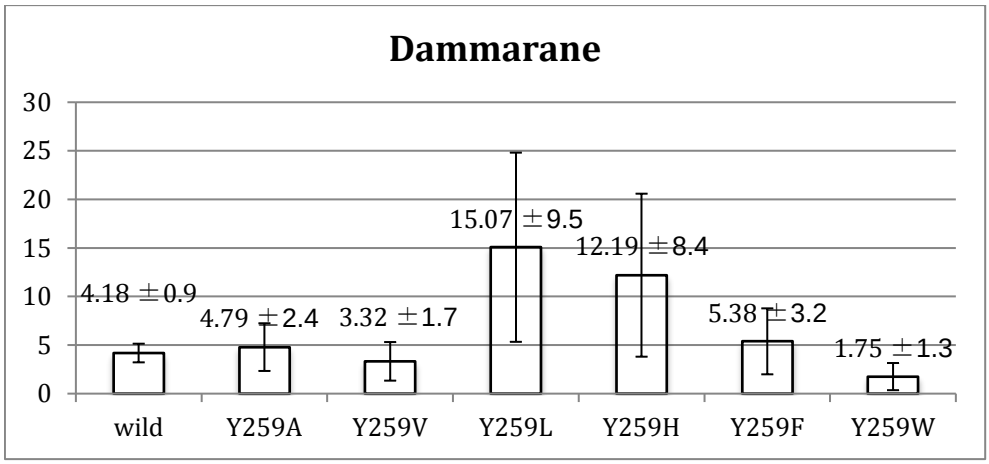

Fig. S10.7. Enzyme activities of the mutants relative to that of the wild-type. These enzyme activities were estimated by dividing the amounts of tetracyclic products **11**, **13**, **14**, **15**, **17** and **19** by the expressed quantities of EtAS enzymes.

Fig. S11. Estimation of the EtAS enzyme activities for the W257X mutants.

<Expression level of β–amyrin synthase (EtAS)>

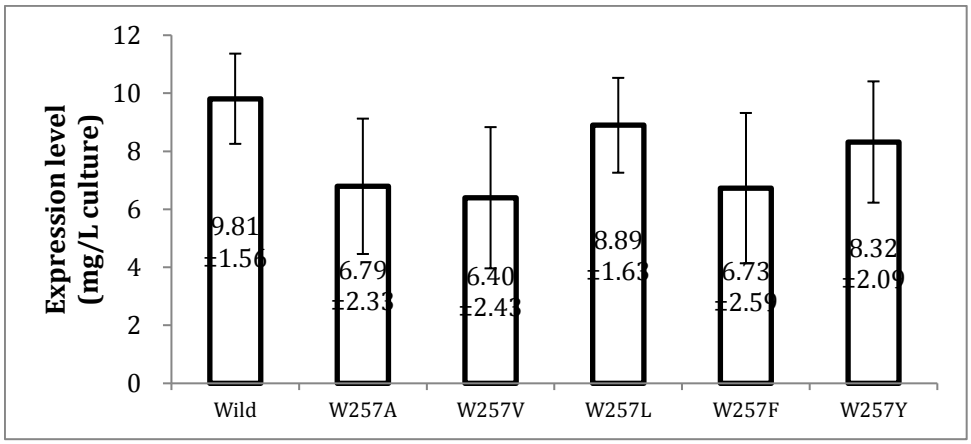

Fig. S11.1. Expression level of β-amyrin synthase (EtAS) for the wild-type and the mutants. The protein amounts (mg) were quantified by Western blot analysis.

＜GC analyses for the quantities of oleanane-type triterpenes＞

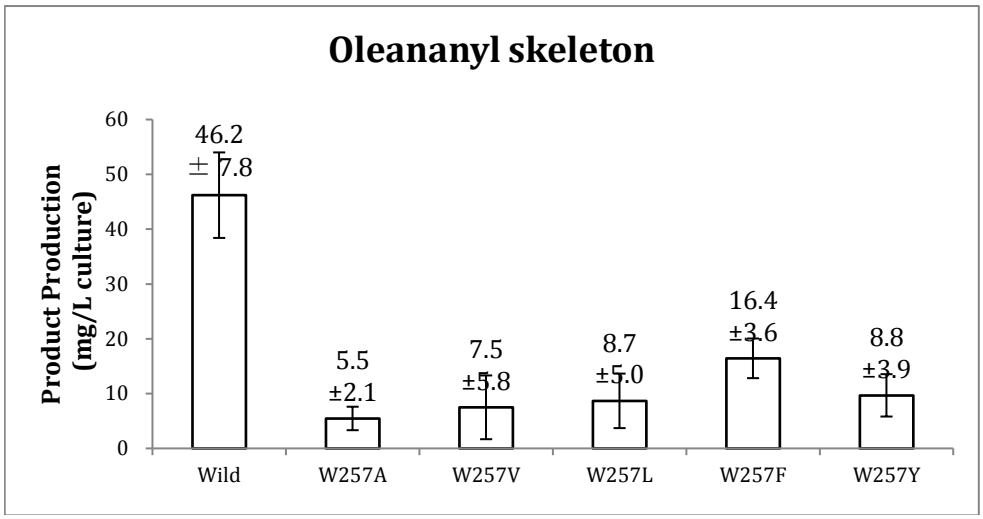

Fig. S11.2. The quantities of oleanyl products (**2** and **16**) for wild-type and the variants, which were determined by GC analyses.

＜Enzyme activities for the production of oleanane-type triterpenes＞

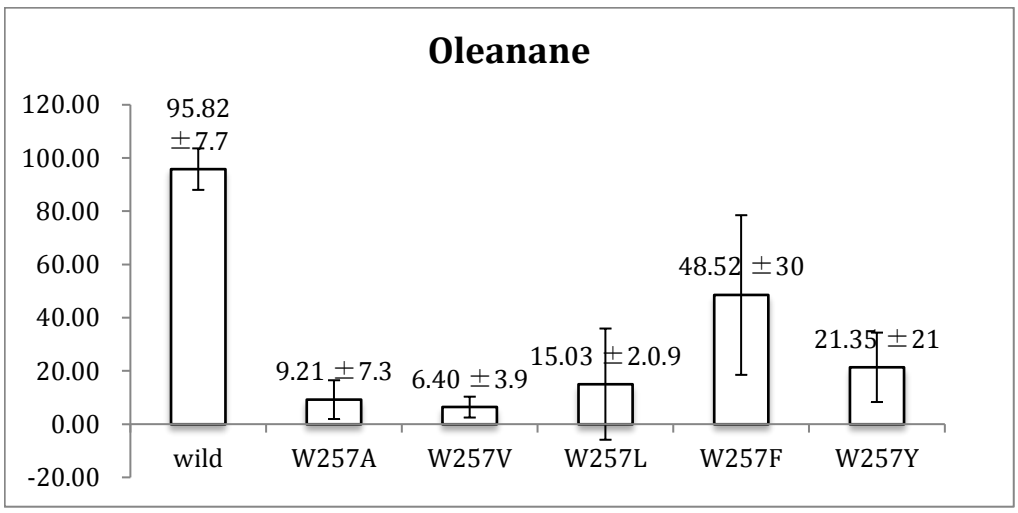

Fig. S11.3. Enzyme activities of the mutants relative to that of the wild-type. These enzyme activities were estimated by dividing the amounts of oleany products **2** and **16** by the expressed quantities of EtAS enzymes.

＜GC analyses for the quantities of lupanyl-type triterpene, lupeol＞

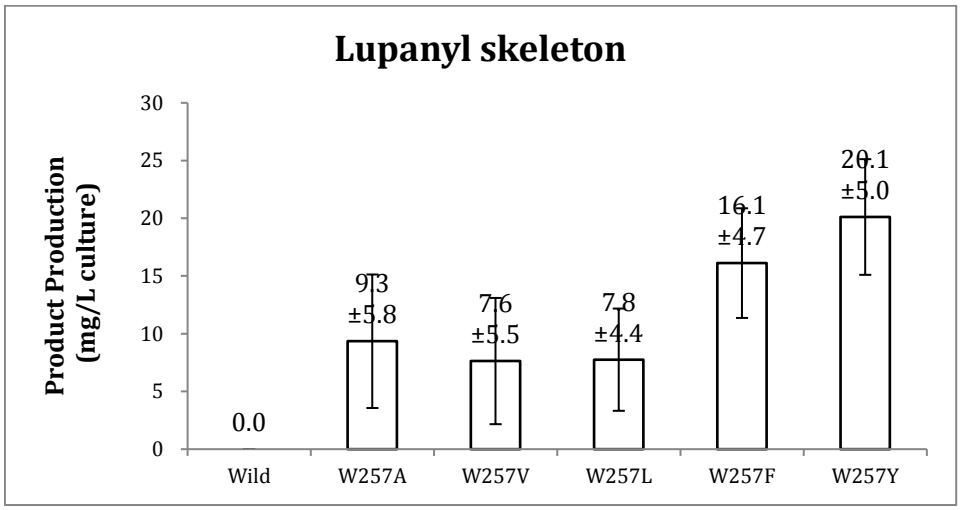

Fig. S11.4. The quantities of lupane skeleton (**20**, lupeol) for wild-type and the variants, which were determined by GC analyses.

＜Enzyme activities for the production of lupeol＞

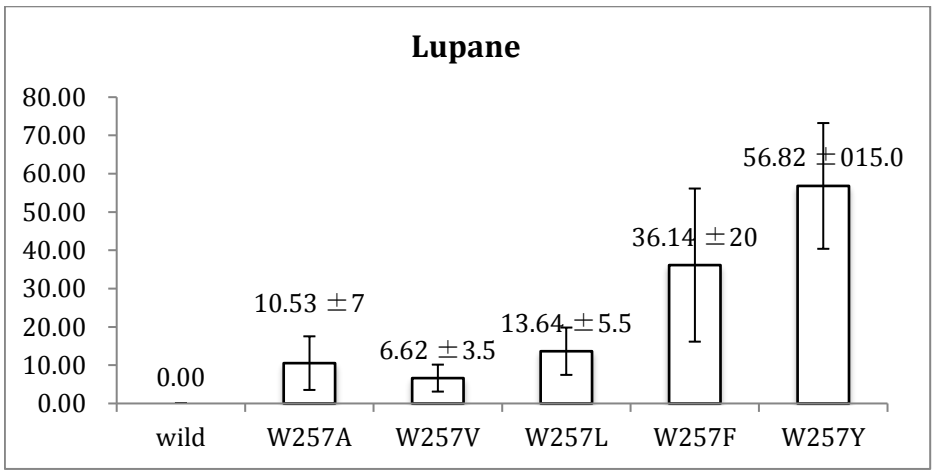

Fig. 11.5. Enzyme activities of the mutants relative to that of the wild-type. These enzyme activities were estimated by dividing the amounts of lupeol **20** by the expressed quantities of EtAS enzymes.

＜GC analyses for the quantities of tetracyclic triterpenes＞

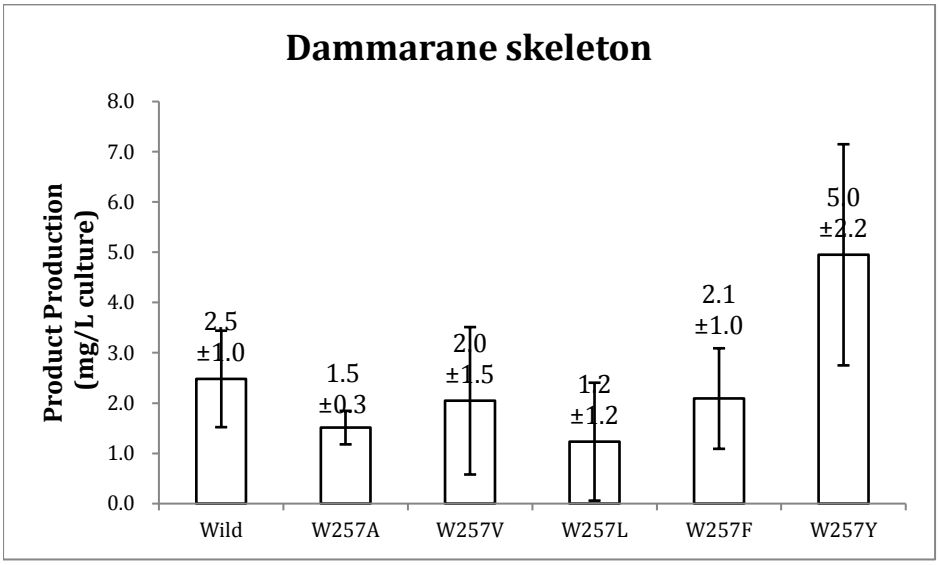

Fig. S11.6. The quantities of dammarenyl skeleton (**13** and **14**) for wild-type and the variants, which were determined by GC analyses.

＜Enzyme activities for the production of dammarenyl skeleton＞

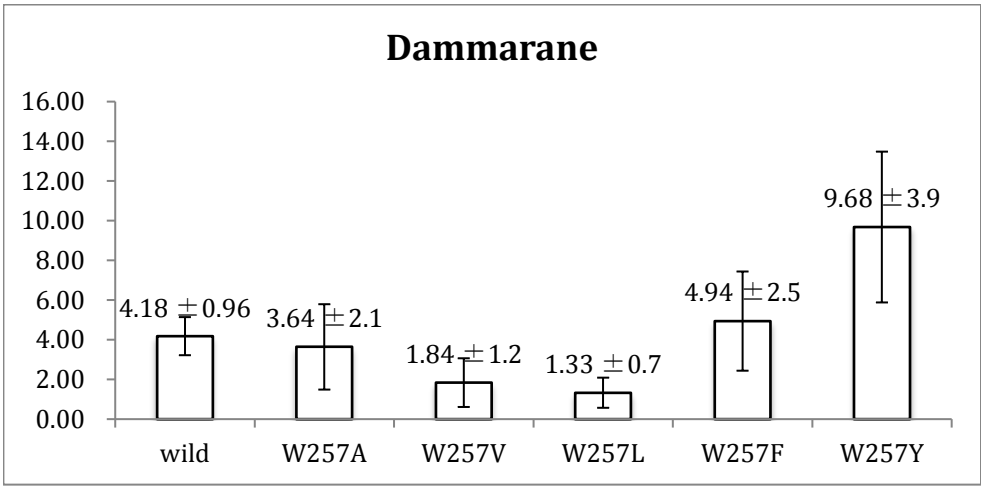

Fig. S11.7. Enzyme activities of the mutants relative to that of the wild-type. These enzyme activities were estimated by dividing the amounts of dammarenyl skeleton (**13** and **14**) by the expressed quantities of EtAS enzymes.